Fuchs, S., Balling, N., Förster, A. (2015): Calculation of thermal conductivity, thermal diffusivity and specific heat capacity of sedimentary rocks using petrophysical well logs. - *Geophysical Journal International*, *203*, 3, pp. 1977—2000.

DOI: http://doi.org/10.1093/gji/ggv403

Geophysical Journal International

Geophys. J. Int. (2015) **203,** 1977–2000 doi: 10.1093/gji/ggv403

GJI Mineral physics, rheology, heat flow and volcanology

Calculation of thermal conductivity, thermal diffusivity and specific heat capacity of sedimentary rocks using petrophysical well logs

Sven Fuchs,[1] Niels Balling[1] and Andrea Förster[2]

[1] *Department of Geosciences, Aarhus University, Høegh-Guldbergs Gade* 2, 8000 *Aarhus C, Denmark. E-mail: fuchs@geo.au.dk*

[2] *Section* 4.1 *Reservoir Technologies, Helmholtz Centre Potsdam, GFZ German Research Centre for Geosciences, Telegrafenberg,* 14473 *Potsdam, Germany*

Accepted 2015 September 18. Received 2015 September 18; in original form 2015 April 24

SUMMARY

In this study, equations are developed that predict for synthetic sedimentary rocks (clastics, carbonates and evapourates) thermal properties comprising thermal conductivity, specific heat capacity and thermal diffusivity. The rock groups are composed of mineral assemblages with variable contents of 15 major rock-forming minerals and porosities of 0–30 per cent. Petrophysical properties and their well-logging-tool-characteristic readings were assigned to these rock-forming minerals and to pore-filling fluids. Relationships are explored between each thermal property and other petrophysical properties (density, sonic interval transit time, hydrogen index, volume fraction of shale and photoelectric absorption index) using multivariate statistics. The application of these relations allows computing continuous borehole profiles for each rock thermal property. The uncertainties in the prediction of each property vary depending on the selected well-log combination. Best prediction is in the range of 2–8 per cent for the specific heat capacity, of 5–10 per cent for the thermal conductivity, and of 8–15 for the thermal diffusivity, respectively. Well-log derived thermal conductivity is validated by laboratory data measured on cores from deep boreholes of the Danish Basin, the North German Basin, and the Molasse Basin. Additional validation of thermal conductivity was performed by comparing predicted and measured temperature logs. The maximum deviation between these logs is $<3\ ^{\circ}$C. The thermal-conductivity calculation allowed an evaluation of the depth range in which the palaeoclimatic effect on the subsurface temperature field can be observed in the North German Basin. This effect reduces the surface heat-flow density by 25 mW m^{-2}.

Key words: Downhole methods; Heat flow; Sedimentary basin processes; Heat generation and transport; Europe.

1 INTRODUCTION

Knowledge on the temperature field of the Earth's subsurface is paramount in the quantification of geological processes and in the exploration of resources, such as hydrocarbons and geothermal energy. In the quantification of the Earth's temperature field, rock thermal properties, such as thermal conductivity (TC), thermal diffusivity (TD) and specific heat capacity (SHC), are essential prerequisites. In particular, when temperature data measured in boreholes are scarce, numerical thermal models are generated at local as well as regional scale for which rock TC forms an important input parameter. Knowledge of rock thermal properties also is prerequisite for quantifying temperature changes in time, as they occur during stimulated heat transfer (extraction of geothermal energy, energy storage, etc.) or during palaeoclimatic temperature changes recorded in the subsurface. As the availability of subsurface rock samples on which rock thermal properties can be measured in the laboratory is generally limited to some geological target formation, the quality of parametrization of thermal models beyond these formations also is limited. Thus, the quality of input data into thermal models often falls behind the capabilities of the numerical tools applied, introducing considerable uncertainty in the modelling results. Insufficient knowledge of temperatures and rock thermal properties of an area, accompanied by a lack of heat-flow values (another important model input parameter) determined from these parameters, causes problems of significance of the thermal models and may result in misinterpretations of the thermal subsurface conditions. In addition, point-scale data from drill cores make an upscaling to representative formation values difficult, in particular for heterogeneous lithologies. It is therefore important to develop methodologies that allow portraying subsurface rock thermal properties from geophysical well logging with a similar degree of resolution as known for the borehole lithology.

Several approaches are available for an indirect determination of TC of sedimentary rocks. For a detailed discussion on the pros and cons of well-log derived TC see Fuchs & Förster (2014). The major shortcoming of most of these methods lies in the fact that the prediction equations for TC are only tested for rocks and regions

for which they are developed. In experimental studies, correlations between thermal and other petrophysical properties are always determined by the specific conditions of the sampled data set. The compositional variation of rock sample sets affects the interrelations between thermal and other petrophysical and thermal rock properties. Therefore, using a specific collection of rock data does not allow to develop equations that are applicable for all sedimentary rocks. Consequently, most researchers limited the applicability of empirical equations to the specific rock types and the region in which the rocks have been sampled. To overcome this limitation, Fuchs & Förster (2014) established prediction equations (for matrix TC) considering a universally comprehensive data set of synthetic rocks that reflects the general variability of sedimentary rock compositions. These equations then can be used for different combinations of well logs and descriptors (bulk density, volume fraction of shale, neutron porosity, sonic transit time and photoelectric absorption index) of up to five standard petrophysical well-log types, depending on their availability. The equations (one equation for each combination of well-log record/descriptor) were developed for three large sets of synthetic 'rocks' of different composition, each representing one of the major groups of sedimentary rocks (clastic rocks, carbonates and evaporites).

The application of the equations by Fuchs & Förster (2014) requires a matrix well-log response value computed from the ordinary bulk well-log response and the well-log derived porosity. Porosity logs are also required to subsequently compute a bulk TC from the predicted matrix TC value, limiting applicability when wells with no porosity log are to be implemented in a study.

The development of well-log based prediction equations for TD and SHC of sedimentary rocks, as far as we know, has not been addressed in recent literature. Some specific prediction equations for SHC are either limited to specific lithotypes or to parameters beyond the scope of modern well logging (e.g. carbon percentage in coals: van Krevelen 1961; volatile-matter content and temperature of coal: Richardson 1993; *cf.* review by Waples & Waples 2004). Beyond these possibilities, TD or SHC basically are calculated from (1) the volume fraction of the rock components by applying some mixing model, (2) the relation between TC, TD, SHC and density and (3) empirical relationships between TC, TD and/or SHC (e.g. Bullard 1954; Von Herzen & Maxwell 1959; Hyndman *et al*. 1979; Goto & Matsubayashi 2008—all for marine sediments).

This paper addresses the lack of a universally applicable well-log based prediction of TC, TD, and SHC for sedimentary rocks in continental sedimentary basins. The approach of Fuchs & Förster (2014), originally intended to compute TC, is improved by considering a variable porosity (ranging between 0 and 30 per cent as typical for rocks in mature continental basins) and applied to all three thermal properties. Bulk values of rock properties are calculated considering the combined effect of mineral matrix and pore-filling fluid (water) and form the basis of the statistical analysis, which finally result in the formulation of refined prediction equations for TC and equations for SHC and TD.

The approach allows predicting profiles of bulk TC, TD and SHC for full borehole sections, directly from the conventional petrophysical well-log records without an intermediate step consisting of the calculation of a matrix well-log response. As this is the first general approach to a TD and SHC prediction based on standard well logs, the study specifically aims at answering the following critical questions: (1) are there statistically significant relations of TD and SHC with other petrophysical properties (here as resolved by logging) and (2) what are the most valuable well-log parameters for the prediction of TD and SHC?

To validate and crosscheck the resulting equations, we compiled a large set of borehole data from three different continental sedimentary basins. Validation is pursued by comparing predicted with laboratory-measured bulk TC and by comparing modelled and measured subsurface temperatures from different borehole locations in northern and central Europe. Results with the new equations for bulk TC are compared with those from the approach by Fuchs & Förster (2014), in which predicted matrix TC was transformed into bulk TC by applying mixing models for a two-phase rock (matrix plus water-filled porosity). Due to the lack of measured TD and SHC data, calculated profiles are validated indirectly by data on rock density. Finally, thermal properties predicted in 0.5-m depth intervals are used to determine average values for geological formations, exemplarily shown for the Hannover location. The application of the well-log based TC calculation allowed for the first time an evaluation of the depth range in which the palaeoclimatic effect on the subsurface temperature field can be observed in the North German Basin.

2 BACKGROUND AND GOVERNING EQUATIONS

2.1 Thermal parameters

In this paper, we use λ for TC [in W (m K)$^{-1}$] and H for the radiogenic heat production (RHP) [in μW m^3] in the calculation of steady-state geothermal conditions (i.e. crustal temperature field), and α for TD [in 10^{-6} m^2 s^{-1}] and c for SHC [in J (kg K)$^{-1}$] in the calculation of transient geothermal conditions (response of a rock body to a transient heat source or sink).

Thermal conductivity, TD and SHC are interrelated by:

$$\alpha = \frac{\boldsymbol{\lambda}}{\rho c}, \tag{1}$$

where ρ is the density (in kg m^{-3}). The basic equation for the conductive heat transport (reads for 1-D) has the mathematical formulation of:

$$\rho c \frac{\partial T}{\partial t} = \frac{\partial}{\partial z}\left(\boldsymbol{\lambda} \frac{\partial T}{\partial z}\right) + H. \tag{2}$$

Here, $\partial T/\partial t$ is the change of temperature with time, $\partial T/\partial z$ is the change of temperature with depth z (also referred in 3-D gradT). For steady-state conditions ($\partial T/\partial t = 0$), eq. (2) simplifies to

$$\frac{\partial}{\partial z}\left(\boldsymbol{\lambda} \frac{\partial T}{\partial z}\right) = -H. \tag{3}$$

The RHP can be calculated from the measured contents of Th, U, K and the density of a rock using relationships given in Rybach (1986) or estimated from gamma-log readings (Bücker & Rybach 1996). Both approaches allow the calculation of the RHP with no lithological limitations and, depending on data quality, typically with an error of $<$10 per cent. The RHP in the crust, in particular from the upper part of the crystalline crust, contributes significantly to the heat flow into sedimentary basins and thus to the heat-flow density as observed near the Earth´s surface.

Heat-flow density (HFD, q in mW m^{-2}) is given by the Fourier's first law (Fourier 1822):

$$\boldsymbol{q} = -\boldsymbol{\lambda}\ \mathrm{gradT}. \tag{4}$$

Table 1. Petrophysical properties and logging-tool characteristic readings of rock-forming minerals typical in sedimentary rocks and of fluids.

Class	Name	κ 10^{-6} m^2 s^{-1}	c J (kg K)$^{-1}$	λ W (m K)$^{-1}$	ρ g cm^{-3}	U barns cm^{-3}	Φ_N p.u.	ΔT µs m^{-1}	γ API
Carbonates	Dolomite	2.16[r]	870[l]	5.4[b,e,f,g]	2.88[a]	9[a]	0.02[a]	140[a,d]	0
	Calcite	1.62[p]	820[n]	3.4[b,e,f,g]	2.71[a]	13.77[a]	0[a]	153[a]	0
Clays	Kaolinite	1.15[r]	974[k]	2.7[b,e]	2.42[a]	6.17[a]	0.37[a]	211[i]	80
	Montmorillonite	1.09[r]	799[q]	1.85[b,e]	2.12[a]	4.3[a]	0.12[a,i]	212[i]	150
	Illite	0.82[r]	796[q]	1.8[b]	2.75[a,c]	11.05[a]	0.2[a]	211[i]	250
Feldspats	Orthoclase	1.28[p]	628[m]	2.25[f,b,e]	2.57[c]	7.5[a]	−0.02[a]	233[a]	220
	Albite	1.08[p]	730[l]	2[f]	2.62[a]	4.35[a]	−0.01[a]	165[a,d,i]	0
	Anorthite	0.82[p]	711[m]	1.9[e]	2.74[a]	8.58[a]	−0.02[a]	145[f]	0
Halogenides	Sylvite	4.45[r]	965[k]	8.5[e]	1.98[a]	15.83[a]	−0.02[a]	242[i]	747
	Halite	3.3[r]	916[k]	6.5[f]	2.15[a]	9.48[a]	−0.02[a]	229[a]	0
Micas	Muscovite	1.03[o]	760[d]	2.33[d,f]	2.82[a]	7.33[a]	0.19[a,i]	151[a,d,i]	270
	Biotite	0.87[r]	770[d]	2[f]	3[a]	19.8[a]	0.21[a]	195[d]	200
Oxides	Quartz	3.8[p]	740[l]	7.7[b]	2.65[a]	4.79[a]	−0.02[a]	182[a]	0
Sulfates	Anhydrite	2.77[r]	585[l]	4.8[f,e,g]	2.96[a]	14.93[a]	−0.02[a]	164[a,i,e]	0
	Gypsum	0.52[r]	1070[l]	1.3[e]	2.32[a]	9.37[a]	0.49[a]	174[g]	0
Fluid	air	19	1004	0.03[j]	0.0012	–	0	3021[e]	–
	water	0.13	3993	0.6[h]	1.1	0.96	1.05	620[a]	–

Notes: Response values at ambient conditions. Values are taken from: [a]Serra (1984); [b]Brigaud & Vasseur (1989); [c]Fertl & Frost (1980); [d]Schön (1996); [e]Schön (1983); [f]Horai (1971); [g]Čermák & Rybach (1982); [h]Lemmon *et al.* (2005); [i]Crain (2013); [j]Gröber (1955); [k]Waples & Waples (2004); [l]Mel'nikova *et al.* (1975); [m]Dortman (1976); [n]Drury *et al.* (1984), [o]Drury (1987); [p]Goto & Matsubayashi (2009); [q]Skauge *et al.* (1983); [r]Calculated from SHC, RHO and TC following eq. 1.

Assuming conduction as main heat transfer process, the subsurface temperature can be modelled (1-D) at any depth based on known heat-flow and TC profiles using:

$$T = T_0 + \sum_{i=z_0}^{z} \frac{\boldsymbol{q}_i}{\boldsymbol{\lambda}_i}, \tag{5}$$

where T is the temperature (in °C) at depth z_i (in m) and T_0 is the temperature at reference depth z_0 (e.g. surface).

2.2 Employed well-log parameters and petrophysical mixing models

We used standard well-log parameters (bulk density: ρ_b, natural gamma-ray: γ, sonic interval transit time: ΔT, hydrogen index [neutron porosity]: ϕ_N, photoelectric absorption index: U) and the volume fraction of shale (V_{sh}), as petrophysical descriptors (Table 1). Usually, the total geophysical tool response (L_{total}) is given by the volume fraction of different components (minerals and fluid contained in pores, V_i). For the theoretical tool response (L_i), the sum of the volume fractions is equal to 1. For any 'user-defined rock composition', the total log response for ρ_b, U, ϕ_N and in the laminated case ΔT (see Savre 1963; Doveton & Cable 1979; Serra 1984) can be calculated by

$$L_{total} = \sum_{1}^{n} V_i L_i. \tag{6}$$

Typical log-response values of minerals and fluids, valid for ambient conditions, are listed in Table 1. The gamma-ray tool response GR (γ) is a function of the radioactivity of the minerals (A_i), the density of the radioactive minerals (ρ_i), their percentage of volume (V_i) and the bulk density (ρ_b) of the rock (Serra 1984):

$$\gamma = \frac{\sum_1^n \rho_i V_i A_i}{\rho_b}. \tag{7}$$

In this study, the volume fraction of shale (V_{sh}, or more precisely the gamma-ray index) is approximated from the gamma-ray readings by the linear relation (Serra 1984):

$$V_{sh} = \frac{\gamma - \gamma_{min}}{\gamma_{max} - \gamma_{min}}, \tag{8}$$

where γ is the gamma-log reading, γ_{min} is the log reading in a clay-free zone, γ_{max} the log reading in a pure-clay zone.

Different models were previously presented for the calculation of thermal properties in a two-phase (solid and pore fluid) system. The geometric-mean model, originally introduced by Lichtenecker (1924), is used to calculate matrix TC (λ_{ma}) from the TC of the mineral constituents (eq. 9, e.g. Merkel *et al.* 1976; Brigaud & Vasseur 1989), where V_i is the volume fraction of each component, and to calculate the water-saturated bulk TC (λ_b) using the matrix TC and porosity (Φ; e.g. Fuchs *et al.* 2013):

$$\boldsymbol{\lambda}_{ma} = \prod_{1}^{n} \boldsymbol{\lambda}_i^{V_i}, \tag{9}$$

where V_i is the volume fraction of each component,

$$\boldsymbol{\lambda}_b = \boldsymbol{\lambda}_{ma}^{1-\phi}\, \boldsymbol{\lambda}_p^{\phi}, \tag{10}$$

where λ_p is the TC of the pore-filling fluid.

The arithmetic-mean model, originally introduced by Voigt (1928) and Reuss (1929), is used to calculate the matrix (volumetric) SHC ($\rho_{ma}c_{ma}$, eq. 11) from the mineral constituents (Drury *et al.* 1984), as well as to calculate the saturated bulk SHC ($\rho_b c_b$, eq. 12) using the matrix SHC and porosity (referred as V_p in eq. 12) (García *et al.* 1991):

$$\rho_{ma}c_{ma} = \sum_{1}^{n} V_i \rho_i c_i \tag{11}$$

$$\rho_b c_b = V_{ma}\rho_{ma}c_{ma} + V_p \rho_p c_p, \tag{12}$$

where V is the volume fraction, ρ is the density and c is the SHC for the rock matrix 'ma', for the pore-filling fluid 'p', and for each

Table 2. Groups of sedimentary rocks with respect to their assumed rock composition, and the min-max range of the particular minerals.

		Range		
Class	Mineral	Carbonates (per cent)	Clastic rocks (per cent)	Evaporites (per cent)
Oxides	Quartz	0–50	50–100	–
	Anorthite	–	0–50	–
Feldspars	Albite	–	0–50	–
	Orthoclase	–	0–50	–
Micas	Muscovite	–	0–20	–
	Biotite	–	0–20	–
Clays	Kaolinite	0–70	–	–
	Montmorillonite	0–70	0–100	–
	Illite	0–70	0–100	–
Carbonates	Calcite	0–100	0–20	0–100
	Dolomite	0–100	0–20	0–100
Sulfates	Anhydrite	–	0–20	0–100
	Gypsum	–	–	0–100
Chlorides	Halite	–	–	0–100
	Sylvite	–	–	0–100

mineral component '*i*', respectively. The term $\rho_{ma}c_{ma}$ (eqs 11 and 12), which is SHC by unit volume of the rock, is also referred to thermal capacity.

The matrix TD of an *n*-mineral component system also is calculated using the geometric-mean model eq. (9) (Goto & Matsubayashi 2009). These authors also deduced a mathematic expression for the saturated bulk TD (eq. 13) implementing eqs (9) and (10) and by introducing f and β as new variables:

$$\kappa_b = f\alpha_p^{\phi}\,\alpha_{ma}^{1-\phi}, \tag{13}$$

where f and β are defined as follows:

$$f = \frac{\beta^{\phi}}{1+(\beta-1)\,\phi} \tag{14}$$

$$\beta = \frac{\rho_p c_p}{\rho_{ma} c_{ma}}. \tag{15}$$

3 WORKFLOW FOR DERIVING PREDICTION EQUATIONS

A synthetic data set of matrix compositions is generated following the approach by Fuchs & Förster (2014). These multi-mineral rock matrix compositions are defined by stepwise combination (in steps of 10 per cent) of different rock-forming minerals common in sedimentary rocks. For clastic rocks and carbonates, this procedure is performed as long as each mineral listed in Table 2 is combined with other minerals within the defined limitations. For marine evaporites, multimineral rock matrix compositions are defined by a stepwise combination of two sequential minerals of the evapouration sequence at a time (calcite–dolomite–gypsum–anhydrite–halite–potassium–magnesium–salt). Then, petrophysical properties are calculated for each mineral combination using the data given in Table 1 and the equations discussed in Section 2.2. These petrophysical properties of the matrix minerals are transformed into bulk-rock values considering variable porosity. The porosity variation (in the range between 0 and 30 per cent) was performed in 5 per cent steps. The resulting bulk-rock values finally formed the basis of the development of TC, TD and SHC prediction equations by multiple regression analysis. The data involved in this statistical analysis are as follows—clastic rocks: regression set: $n = 151\,021$, test set: $n = 37\,755$; carbonates: regression set: $n = 15\,764$, test set: $n = 3934$; evapourates: regression set: $n = 286$, test set: $n = 71$, respectively.

Nine data sets (three different rock thermal properties for each of the three major sedimentary rocks groups) are examined in total. Each data set is randomly subdivided into two groups, a set of 'regression' data (80 per cent of total data) and a set of test data (remaining 20 per cent). The 'regression'-data set is used for the statistical analysis and derivation of prediction equations, while the test data set is used to test the statistical quality of the prediction equations. Simple linear regression (SLR) and multiple linear regression (MLR), based on a least-squares estimation, are applied to predict the values on a quantitative outcome variable (dependent variables: TC, TD or SHC) using one or more predictor variables (independent variables: well-log values). The performance of the applied methods is evaluated by regression subset (values not reported) and test subset (reported fitting data) by calculating the arithmetic mean error (ame), the root mean square error (rms), the coefficient of variation (cv), and the adjusted coefficient of determination (R^2) between predicted and measured values, respectively. Prediction errors are always calculated based on the absolute deviations between predicted and measured values. The statistical approach is the same as described in Fuchs & Förster (2014). Further details on the statistical methods and parameters applied are described, for instance, by Deutsch & Journel (1998).

In geothermal studies, the well-log database available for an indirect prediction of thermal properties is generally quite heterogeneous. Therefore, we derive regression prediction equations for any possible combination of the standard well logs applied. This enables the user to select and apply the equations with the smallest prediction error for log combinations possible and suitable in each case. In the Appendix, information on the regression coefficients, some selected statistical parameters, and the prediction errors (for synthetic data set) are provided for all thermal properties (TC, TD and SHC). Comprehensive statistical information on the uncertainties are summarized in the electronic supplemental as Table T1–T3. The total number of possible log combination included sums up to 15 equations (#1–#15) for evaporites (no intrinsic natural gamma response result in reduced number of equations) and to 31 equations for carbonate (#16–#46) and 41 for clastic rocks (#47–#77), respectively. However, to achieve a large explained variance (minimising the prediction error), that is by selecting an 'optimal log configuration', we recommend the use of the 'best' empirical equations for each rock group and thermal property as described in the following subsections (Table 3, Fig. 1).

4 RESULTS

4.1 TC prediction for synthetic rock compositions

4.1.1 Evaporites

Applying SLR, the largest explained variance is observed for the hydrogen index ($R^2 = 0.741$), while the ρ_b and ΔT show poor predictor capabilities ($R^2 < 0.02$). Using two predictor variables in MLR the combinations of ρ_b and ϕ_n surprisingly results in the largest explained variance observed ($R^2 = 0.903$) and in a smaller ame (11.4 ± 11 per cent) as to be expected. Additional predictor variables only insignificantly improve the TC predictions. Therefore, the combination of ρ_b and ϕ_n is recommended to predict bulk TC in evaporites (Table 3, eq. A5).

Table 3. Best-fitting prediction equations of thermal rock properties for variable number of predictor variables (well logs).

Parameter	Rock group	No. of predictor variables	#	Prediction equations* [W/(mK)]	Error calculation: Artificial validation set R^2 [per cent]	Artificial validation set Mean [per cent]	Artificial validation set SD [per cent]	Subsurface data set Mean [per cent]	Subsurface data set SD [per cent]	Subsurface data set Rms [per cent]
Thermal conductivity	Evaporites	1	A2	$\lambda = 5.34 - 8.14\,\phi_N$	74%	18.0%	14.5%			
		2	A5	$\lambda = 10.73 - 2.22\,\rho_b - 9.21\,\phi_N$	90%	11.4%	11.0%			
		3	A12	$\lambda = 14.4 - 3.16\,\rho_b - 8.97\,\phi_N - 0.0063\Delta T$	92%	11.2%	9.7%	no data available		
		4	A15	$\lambda = 14.32 - 3.15\,\rho_b - 8.93\,\phi_N + 0.005U - 0.0063\Delta T$	92%	11.2%	9.8%			
	Carbonates	1	A17	$\lambda = 3.92 - 5.11\,\phi_N$	59%	13.6%	10.4%			
		2	A30	$\lambda = 5.84 - 0.0063\Delta T - 1.48 V_{sh}$	77%	9.8%	7.2%			
		3	A35	$\lambda = -4.37 + 4.18\,\rho_b - 0.3\,U - 1.45 V_{sh}$	91%	6.4%	4.9%	no data available		
		4	A44	$\lambda = 0.33 + 2.73\,\rho_b - 0.28\,U - 0.0056\Delta T - 1.54 V_{sh}$	93%	5.4%	4.5%			
		5	A46	$\lambda = 1.15 + 2.59\,\rho_b + 1.08\,\phi_N - 0.28\,U - 0.0083\Delta T - 1.66 V_{sh}$	94%	5.2%	4.6%			
	Clastics	1	A48	$\lambda = 3.41 - 4.83\,\phi_N$	51%	15.4%	11.2%	18.9%	11.1%	21.9%
		2	A58	$\lambda = 4.17 - 3.89\,\rho_b - 1.78 V_{sh}$	76%	11.0%	8.8%	16.7%	10.2%	19.6%
		3	A67	$\lambda = 3.66 - 5.13\,\phi_N + 0.0029\Delta T - 1.70 V_{sh}$	76%	11.0%	8.7%	15.8%	9.7%	18.6%
		4	A74	$\lambda = -1.55 + 1.39\,\rho_b - 6.81\,\phi_N + 0.0115\Delta T - 1.53 V_{sh}$	79%	10.4%	8.1%	15.2%	10.8%	18.6%
		5	A77	$\lambda = -3.6 + 2.42\,\rho_b - 5.84\,\phi_N - 0.1\,U - 0.0113\Delta T - 1.32 V_{sh}$	80%	10.2%	8.1%	15.6%	11.5%	19.4%
Thermal diffusivity	Evaporites	1	B2	$\lambda = 2.49 - 4.35\,\phi_N$	73%	25.2%	27.9%			
		2	B5	$\lambda = 4.94 - 1.01\,\rho_b - 4.84\,\phi_N$	84%	21.8%	23.5%			
		3	B12	$\lambda = 7.83 - 1.75\,\rho_b - 4.65\,\phi_N - 0.0050\Delta T$	87%	19.6%	19.5%	no data available		
		4	B15	$\lambda = 6.86 - 1.70\,\rho_b - 4.16\,\phi_N + 0.065U - 0.0046\Delta T$	88%	19.0%	19.6%			
	Carbonates	1	B17	$\lambda = 1.83 - 2.95\,\phi_N$	77%	12.4%	9.2%			
		2	B30	$\lambda = 2.88 - 0.0063\Delta T - 0.44 V_{sh}$	81%	10.9%	7.8%			
		3	B40	$\lambda = 4.02 - 0.092\,U - 0.0080\Delta T - 0.57 V_{sh}$	91%	7.9%	6.9%	no data available		
		4	B44	$\lambda = 2.12 + 0.65\,\rho_b - 0.113\,U - 0.0061\Delta T - 0.52 V_{sh}$	92%	7.1%	6.4%			
		5	B46	$\lambda = 1.59 + 0.57\,\rho_b - 0.70\phi_N - 0.113\,U - 0.0043\Delta T - 0.45 V_{sh}$	92%	7.1%	6.2%			
	Clastics	1	B48	$\lambda = 1.69 - 3.09\,\phi_N$	67%	15.7%	11.3%			
		2	B58	$\lambda = 1.95 - 2.77\,\phi_N - 0.60 V_{sh}$	77%	14.0%	10.9%	no data available		
		3	B66	$\lambda = 2.06 - 2.86\,\phi_N - 0.016U - 0.55 V_{sh}$	77%	13.9%	10.9%			
		4	B72	$\lambda = -2.62 + 1.65\,\rho_b - 3.32\,\phi_N - 0.116U + 0.0049\Delta T$	77%	13.8%	10.4%			
		5	B77	$\lambda = -0.79 + 1.10\,\rho_b - 2.55\phi_N - 0.08\,U + 0.002\Delta T - 0.38 V_{sh}$	79%	13.3%	10.4%			
Specific heat capacity	Evaporites	1	C4	$\lambda = 54.08 + 5.19\Delta T$	69%	13.0%	9.9%			
		2	C10	$\lambda = 991.1 - 73.54\,U + 4.37\Delta T$	87%	6.9%	7.1%			
		3	C14	$\lambda = 640.4 + 580.3\phi_N - 44.69\,U + 4.07\Delta T$	92%	6.1%	4.9%	no data available		
		4	C15	$\lambda = -231.7 + 245.2\,\rho_b + 585.8\phi_N - 42.88\,U + 5.23\Delta T$	93%	6.0%	4.5%			
	Carbonates	1	C19	$\lambda = -376.7 + 6.75\Delta T$	92%	5.9%	5.0%			
		2	C30	$\lambda = -316.7 + 7.14\Delta T - 312.8 V_{sh}$	97%	3.5%	3.0%			
		3	C39	$\lambda = 60.69 + 1186\phi_N + 4.63\Delta T - -422.5 V_{sh}$	99%	2.3%	2.0%	no data available		
		4	C43	$\lambda = 403.8 - 98.0\,\rho_b + 1253\phi_N + 4.15\Delta T - 439.9 V_{sh}$	99%	2.3%	1.9%			
		5	C46	$\lambda = 584 - 194.4\,\rho_b + 1250\phi_N + 10.93\,U + 4.03\Delta T - 435.9 V_{sh}$	99%	2.2%	1.8%			
	Clastics	1	C50	$\lambda = -592 + 7.25\Delta T$	96%	4.3%	4.0%			
		2	C61	$\lambda = -517.5 + 7.38\Delta T - 196.3 V_{sh}$	98%	3.3%	3.1%			
		3	C67	$\lambda = 59.3 + 1536\phi_N + 3.99\Delta T - 302.1 V_{sh}$	99%	1.8%	1.6%	no data available		
		4	C74	$\lambda = 891.3 - 221.4\,\rho_b + 1804\phi_N + 2.62\Delta T - 329.5 V_{sh}$	100%	1.3%	1.1%			
		5	C77	$\lambda = 814.6 - 182.9\,\rho_b + 1841\phi_N - 3.62\,U + 2.61\Delta T - 321.8 V_{sh}$	100%	1.3%	1.1%			

Note: *A complete overview of all equations can be found in the Appendices A (TC), B (TD) and C (SHC), respectively.

4.1.2 Carbonates

Using SLR, ρ_b, ϕ_n and ΔT (one predictor variable) show the same level of explained variances ($R^2 = 0.57 \pm 0.02$) and expected ame (~13.6 per cent). Any combination of two predictor variables allows the prediction of bulk TC within a mean error between 10 and 13 per cent. The best prediction results from the combination of ΔT and V_{sh} (R^2 of 0.767 and ame of 9.8 per cent) (Table 3, eq. A30). Smaller errors can be achieved only when the photoelectric absorption index U is included in the MLR. The predictive ame then is between 5 and 10 per cent for any possible log combination. Best predictions for carbonates are achieved with ρ_b, U and V_{sh} in a three-predictor equation (eq. A35; ame: 6.4 ± 4.9 per cent) and by additionally including ΔT in a four-predictor equation (eq. A44, ame: 5.4 ±4.5 per cent).

4.1.3 Clastic rocks

For clastic rocks, SLR predicts TC with an average ame not better than 17 per cent. For two-predictor variables the best prediction is clearly given by using log-combinations of V_{sh} with ϕ_n, ΔT or ρ_b (ame: 11–13 per cent). However, increasing the number of logs up to the maximum of five does not decrease the ame to less than

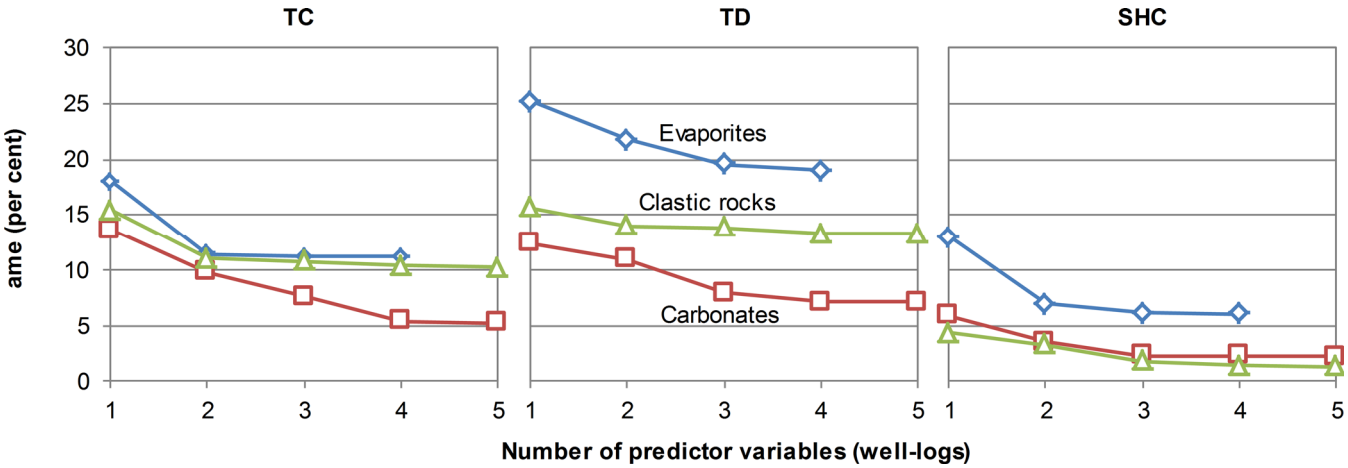

Figure 1. Lowest arithmetic mean error to be expected for the well-log based prediction of TC, TD and SHC.

10 per cent. Even by using all five logs, 20 per cent of the TC variance still remains unexplained. Overall, V_{sh} and ϕ_n seems to be the most powerful combination for bulk TC predictions (Table 3, eq. A 58, $R^2 = 0.762$, ame: 11 ± 8.8 per cent).

4.2 TD prediction for synthetic rock compositions

4.2.1 Evaporites

Applying SLR to the set of evaporite rocks, the largest explained variance is observed for the hydrogen index ($R^2 = 0.728$), while ρ_b and ΔT show only poor predictor capabilities ($R^2 < 0.01$). Using two-predictor variables in MLR, the largest explained variance is given by ρ_b and ϕ_n ($R^2 = 0.843$) resulting in a rather high ame of 21.8 ± 23.5 per cent (Table 3, eq. B5). By adding U and ΔT in the MLR, only minor improvements are observed (maximum $R^2 = 0.883$; minimum ame: 19 ± 19.6 per cent). The combination of ρ_b and ϕ_n is recommended to predict bulk TD in evaporite rocks (Table 3, eq. A5). Errors to be expected are 25–62, 22–60, 20–44 and 19 per cent for one-, two-, three- and four-predictor-variables equations, respectively.

4.2.2 Carbonates

Performing SLR on the carbonate data set, ϕ_n and ΔT provides the highest level of explained variances ($R^2 \sim 0.75$), which allows predicting TD by simple correlation with an average error of 12.5 per cent. The use of two-predictor variables only slightly improves the prediction quality (MLR; best values: $R^2 = 0.809$, ame $= 10.9 \pm 7.8$ per cent). Only by using at least three-predictor variables, the overall ame can be reduced down to *ca*. 7 per cent. By using as few as possible logs at the same time, eq. B40 (Table 3) is recommended to be used for TD prediction. This equation includes ΔT, V_{sh} and U and shows a prediction of bulk TD within a mean error of 7.9 ± 6.9 per cent ($R^2 = 0.906$).

4.2.3 Clastic rocks

For clastic rocks, TD can be predicted applying SLR with a minimum ame of 16 per cent. MLR predicts TD with an average ame not better than 13 per cent. Almost all deduced equations with at least two-predictor variables are able to predict TD with a mean error ranging between 13 and 15 per cent. The two-log-based equation including V_{sh} and ϕ_n (Table 3, eq. B58) is recommended due to the smallest prediction ame of 14 ± 10.9 per cent.

4.3 SHC prediction for synthetic rock compositions

4.3.1 Evaporites

Prediction of SHC for evaporite rocks is possible with a minimum ame of 13 per cent using simple correlations to ΔT ($R^2 = 0.693$) and with a minimum ame of 6 per cent including additional predictor variables. Sufficient prediction quality (ame between 6 and 8 per cent) can be achieved by applying MLR to various two- and three-variable log-combinations, the best of them including ΔT and U.

4.3.2 Carbonates

Using SLR, ΔT shows clearly the highest level of explained variances ($R^2 = 0.92$) and the smallest expected error (ame: 5.9 per cent). The combination of different well logs results in a decreasing mean error with a maximum value of approx. 11 per cent (two-predictor; exception eq. C29), 10 per cent (three-predictors), 5 per cent (four-predictors) and 2 per cent (five-predictors), respectively. The combination of ΔT and V_{sh}, with the small average errors of 3.5 per cent only ($R^2 = 0.973$), is recommended for the prediction of bulk SHC in carbonates (Table 3, eq. C30).

4.3.4 Clastic rocks

For clastic rocks, the same strong correlation between SHC and ΔT ($R^2 = 0.964$) was found as for carbonates. When ΔT is available, reasonable SHC predictions can be achieved by using ΔT only (ame: 4.3 per cent). Otherwise, reliable predictions of SHC in clastic rocks can be made by using log combinations including ϕ_n and MLR (ame: always <5.9 per cent).

4.4 Formation specific values of TC, TD and SHC

Table 4 lists the formation-specific values of TC, TD and SHC, calculated on basis of the well-log based predictions and the stratigraphic profile, in conjunction with the temperature and pressure range for the Hannover well. The calculation of TC is addressed in Section 5.1; profiles of rock thermal properties are partly shown in

Table 4. Mean bulk values for TC, TD and SHC for Cenozoic and Mesozoic formations of the Groß-Buchholz GT1 borehole at the Hannover location in the NGB. Values are not corrected for temperature and pressure *in situ* conditions.

Depth		Stratigraphy	TC	TD	SHC	Temperature	Pressure
Top (m)	Bottom (m)		[W (mK)$^{-1}$]	10^{-6} [m^2 s^{-1}]	[J (kg K)$^{-1}$]	(°C)	(MPa)
0	31	**Quarternary**	**2.85 ± 0.5**	**1.23 ± 0.21**	**1238 ± 6**	**13.3–14.7**	**0–0.8**
–	–	**Tertiary**	–	–	–	–	–
31	1335	**Cretaceous**	**1.8 ± 0.6**	**0.8 ± 0.2**	**1243 ± 95**	15–74	1–34
31	1335	Lower Cretaceous	1.8 ± 0.6	0.8 ± 0.2	1243 ± 95	15–74	1–34
31	270	Albian	1.8 ± 0.2	0.8 ± 0.1	1250 ± 3	15–24	1–7
270	730	Aptian	1.5 ± 0.2	0.6 ± 0.1	1254 ± 2	24–48	7–19
730	830	Barremian	1.4 ± 0.1	0.6 ± 0.1	1254 ± 2	48–53	19–21
830	1070	Hauterivian	1.5 ± 0.2	0.7 ± 0.1	1254 ± 2	53–65	21–27
1070	1140	Valanginian	2 ± 0.4	0.9 ± 0.1	1258 ± 22	65–68	27–29
1140	1335	Berriasian (Wealden)	2.9 ± 0.8	1.1 ± 0.3	1181 ± 237	68–74	29–34
1335	2375	**Jurassic**	**2 ± 0.7**	**0.8 ± 0.3**	**1283 ± 218**	**74–124**	**34–61**
1335	1600	Upper Jurassic (Malm)	2.6 ± 0.8	1.1 ± 0.4	1155 ± 300	74–85	34–41
1335	1415	Tithonian	2.3 ± 0.8	0.9 ± 0.3	1335 ± 197	74–78	34–36
1510	1590	Kimmeridgian	3.3 ± 0.3	1.6 ± 0.2	851 ± 133	82–84	39–41
1590	1600	Oxfordian	2.4 ± 0.5	1 ± 0.3	1389 ± 185	84–85	41–41
1600	1950	Middle Jurassic (Dogger)	1.9 ± 0.7	0.8 ± 0.3	1280 ± 173	85–102	41–50
1600	1675	Callovian	2.2 ± 0.6	0.9 ± 0.3	1240 ± 180	85–88	41–43
1675	1765	Bathonian	2.6 ± 0.6	1.1 ± 0.3	1106 ± 152	88–92	43–45
1765	1860	Bajocian	1.4 ± 0.2	0.6 ± 0.1	1381 ± 88	92–97	45–47
1860	1950	Aalenian	1.4 ± 0.2	0.6 ± 0.1	1383 ± 67	97–102	47–50
1950	2375	Lower Jurassic (Liassic)	1.6 ± 0.3	0.7 ± 0.1	1366 ± 135	102–124	50–61
1950	2100	Toarcian	1.6 ± 0.2	0.6 ± 0.1	1434 ± 80	102–110	50–54
2100	2180	Pliensbachian	1.6 ± 0.2	0.7 ± 0.1	1359 ± 87	110–114	54–56
2180	2290	Sinemurian	1.5 ± 0.2	0.6 ± 0.1	1388 ± 79	114–121	56–58
2290	2375	Hettangian	1.8 ± 0.3	0.8 ± 0.2	1224 ± 191	121–124	58–61
2375	3874	**Triassic**	**3.3 ± 1.5**	**1.6 ± 0.7**	**802 ± 139**	**124–168**	**61–99**
2375	2852	Keuper	2.6 ± 0.4	1.2 ± 0.2	788 ± 147	124–141	61–73
2375	2445	Upper Keuper (Exter-Fm.)	2.2 ± 0.6	1 ± 0.3	915 ± 259	124–127	61–62
2445	2795	Middle Keuper	2.7 ± 0.4	1.2 ± 0.1	770 ± 102	127–138	62–71
2445	2610	Steinmergelk.- Rt. Wand (Arnstadt-/Weser-Fm.)	2.7 ± 0.3	1.2 ± 0.1	749 ± 109	127–132	62–67
2610	2640	Schilfsandstein (Stuttgart-Fm.)	2.5 ± 0.3	1.2 ± 0.1	722 ± 80	132–133	67–67
2640	2795	Lower Gipskeuper (Grabfeld-Fm.	2.7 ± 0.4	1.2 ± 0.2	800 ± 89	133–138	67–71
2795	2852	Lower Keuper	2.6 ± 0.4	1.2 ± 0.1	742 ± 99	138–141	71–73
2795	2878	Lettenkohlenkeuper (Erfurt-Fm.)	2.7 ± 0.4	1.3 ± 0.2	736 ± 104	138–142	71–73
2852	3162	Muschelkalk	4 ± 1.6	1.9 ± 0.8	813 ± 132	141–149	73–81
2852	2878	Upper Muschelkalk (Hauptmuschelkalk-Folge)	2.8 ± 0.5	1.4 ± 0.2	728 ± 116	141–142	73–73
2878	3045	Middle Muschelkalk (Anhydrit-Folge)	5 ± 1.6	2.3 ± 0.8	807 ± 163	142–145	73–78
3045	3162	Lower Muschelkalk (Wellenkalk-Folge)	2.9 ± 0.3	1.3 ± 0.1	840 ± 55	145–149	78–81
3162	3874	Buntsandstein	3.5 ± 1.7	1.7 ± 0.8	806 ± 135	149–168	81–99
3162	3440	Upper Buntsandstein (Röt-Fm.)	4.8 ± 2.1	2.3 ± 1	923 ± 115	149–155	81–88
3440	3705	Middle Buntsandstein	2.8 ± 0.5	1.4 ± 0.2	725 ± 89	155–163	88–94
3440	3527	Solling-Folge	2.5 ± 0.3	1.2 ± 0.2	819 ± 74	155–158	88–90
–	–	Hardegsen-Folge	–	–	–	–	–
3527	3568	Detfurth-Folge	3 ± 0.6	1.5 ± 0.2	706 ± 64	158–159	90–91
3568	3705	Volpriehausen-Folge	2.9 ± 0.4	1.5 ± 0.2	671 ± 46	159–163	91–94
3705	3874	Lower Buntsandstein	2.6 ± 0.5	1.3 ± 0.2	742 ± 78	163–168	94–99
3705	3838	Bernburg-Fm.	2.7 ± 0.5	1.3 ± 0.2	723 ± 72	163–167	94–98
3838	3874	Calvörde-Fm.	2.2 ± 0.3	1.1 ± 0.1	809 ± 57	167–168	98–99

Figs 3, 5, and 6). Due to the lack or ambiguity of appropriate correction equations to convert values from ambient to *in-situ* conditions, the depth-dependent influence of temperature and pressure on TC, TD and SHC are not considered in the calculation. The impact of the lithological variability is reflected in the reported SD.

The lowest TC [<1.5 W (m K)$^{-1}$] is observed for instance in the Aptian, Barremian, Bajocian and Aalenian sections that are dominated by claystones and clayey marlstones; the highest TC [>4.0 W (m K)$^{-1}$] is observed in the Middle Muschelkalk and in some intervals of the Upper Buntsandstein, mainly caused by anhydrite and rock salt. The values of the latter two stratigraphic units exhibit high SD, indicating large lithological variability. The average TC of the whole Triassic [3.33 ± 1.48 W (m K)$^{-1}$] is significantly higher than the average TC of the Lower Cretaceous [1.77 ± 0.61 W (m K)$^{-1}$]. Values for TD show the same pattern as TC, while values for SHC show a reverse pattern (high TC values associated with small SHC values and *vice versa*). The highest SHC is observed in the Jurassic and Cretaceous, especially in the clay-rich formations of the Oxfordian, Bajocian, Aalenian and Toarcian. Considering the prediction quality of the equations applied to

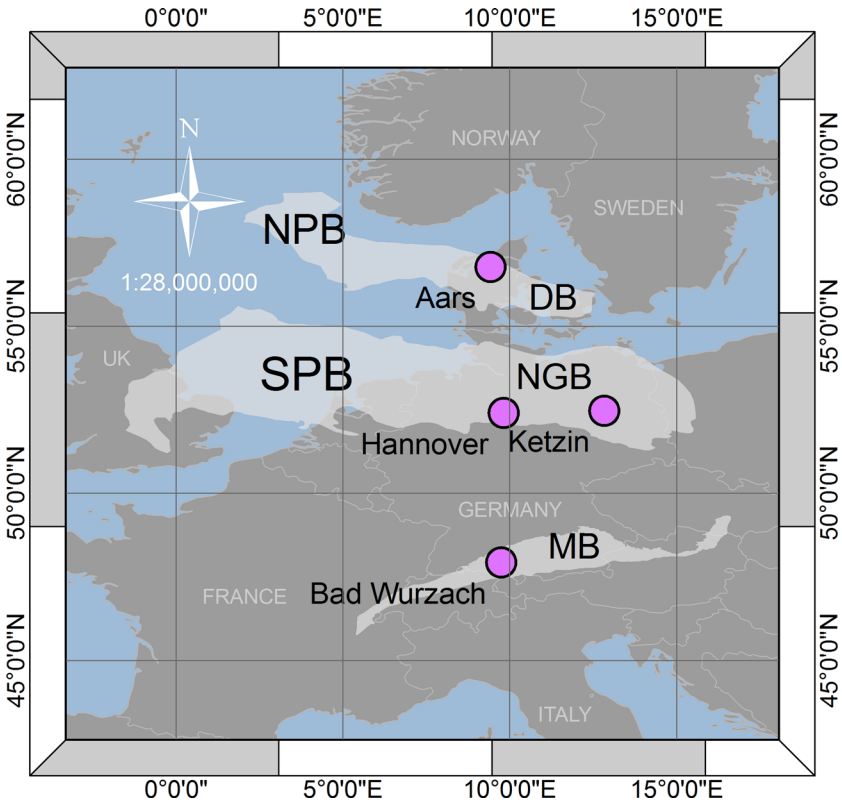

Figure 2. Study area and borehole sites in Northern and Central Europe. Basins: SPB: Southern Permian Basin, NPB: Northern Permian Basin, NGB: North German Basin, DB: Danish Basin, MB: Molasse Basin. Outlines of Permian Basins after Ziegler (1990).

generate the continuous profiles, the uncertainties of the calculated formation thermal parameters are assumed to range between 5 and 46 per cent (median: 12 per cent) for TC, 7 and 60 per cent (median: 15 per cent) for TD and 1 and 25 per cent (median: 3 per cent) for SHC, respectively.

5 VALIDATION

The validation of predicted values of TC, TD, SHC and subsurface-temperature predictions is performed by using a large data set compiled from boreholes of three continental sedimentary basins in central and northern Europe (Fig. 2). The basins differ with regard to basin history and sedimentation. Petrophysical well logs, temperature data and laboratory TC data used are from four wells of the North Germany Basin (NGB), one well of the Danish Basin (DB) and one well of the Molasse Basin (MB), respectively. The NGB data set (site A: Ketzin, 3 wells, max depth: *ca*. 0.8 km; site B: Hannover, 1 well, max. depth: *ca*. 3.9 km) is the same as used before and described in detail by Fuchs & Förster (2014). Additional data from the MB (site C: Bad-Wurzach borehole) are from Hartmann *et al.* (2005) and the State Office of Geology, Raw Materials and Mining in Freiburg (LGRB). The borehole at this site is drilled to a total depth of *ca*. 850 m into a Tertiary Flysch sequence (Upper Marine Molasse formation). Well-log, temperature and laboratory data are available from a cored section between 570 and 810 m depth (with courtesy of Andreas Hartmann, Volker Rath and Christopher Clauser). An extension of the previously used database is made with borehole data from the DB. Well-log data used are from the Aars-1 well, which was drilled to a depth of 3.4 km in the Upper Keuper. A series of high-precision temperature profiles (measured by N. Balling and his group at Aarhus University) are available, and the most recent one from 2014 is used for this study.

5.1 Measured versus predicted TC

Predictions of bulk TC are compared with laboratory-measured TC values from the NGB and the MB data, respectively. This data set, consisting of clastic rocks, allows evaluating eqs A47 to A77 (listed in Appendix A). Average deviations between predicted and measured values are calculated from the absolute deviations, either for specific geological formations or for the full data set (listed in the electronic supplementary material Table T1). One-metre-running averages of well-log based predictions (scale: ∼0.35–0.5 m) and laboratory-measured TC values (scale: ∼0.01 m) are used in the calculation to honor the different scale of well-logs and laboratory measurements. Depth-dependent influences of temperature and pressure are a priori not considered.

In general, the prediction potential of the derived equations varies significantly depending on type and number of the well logs included, and, to a minor extent, on the geological formation. Almost half of the well-log combinations allow predicting TC (full data set) with a mean deviation averaging to about 15 per cent. Remaining equations show larger mean deviations ranging between 15 and 30 per cent. However, most of the equations closely reproduce observed changes in TC along geological sections as shown for two examples in Fig. 3.

For the individual geological formations, the smallest prediction deviations are 5.8 ± 4.5 per cent (A61, Süßwassermolasse, MB), 8.8 ± 5.5 per cent (A77, Middle Buntsandstein, NGB), 10.7 ± 10.3 per cent (A75, Stuttgart Fm., NGB) and 14.0 ± 9.4 per cent (A63, Wealden Fm., NGB). For the full data set, the smallest prediction deviation is obtained by applying eq A76 (including ϕ_n, ΔT, ρ_b and V_{sh}), which allows TC predictions with a mean deviation of 15.0 ± 11.5 per cent (rms = 17.7 per cent). Deviations (mean, rms) for each equation are documented in

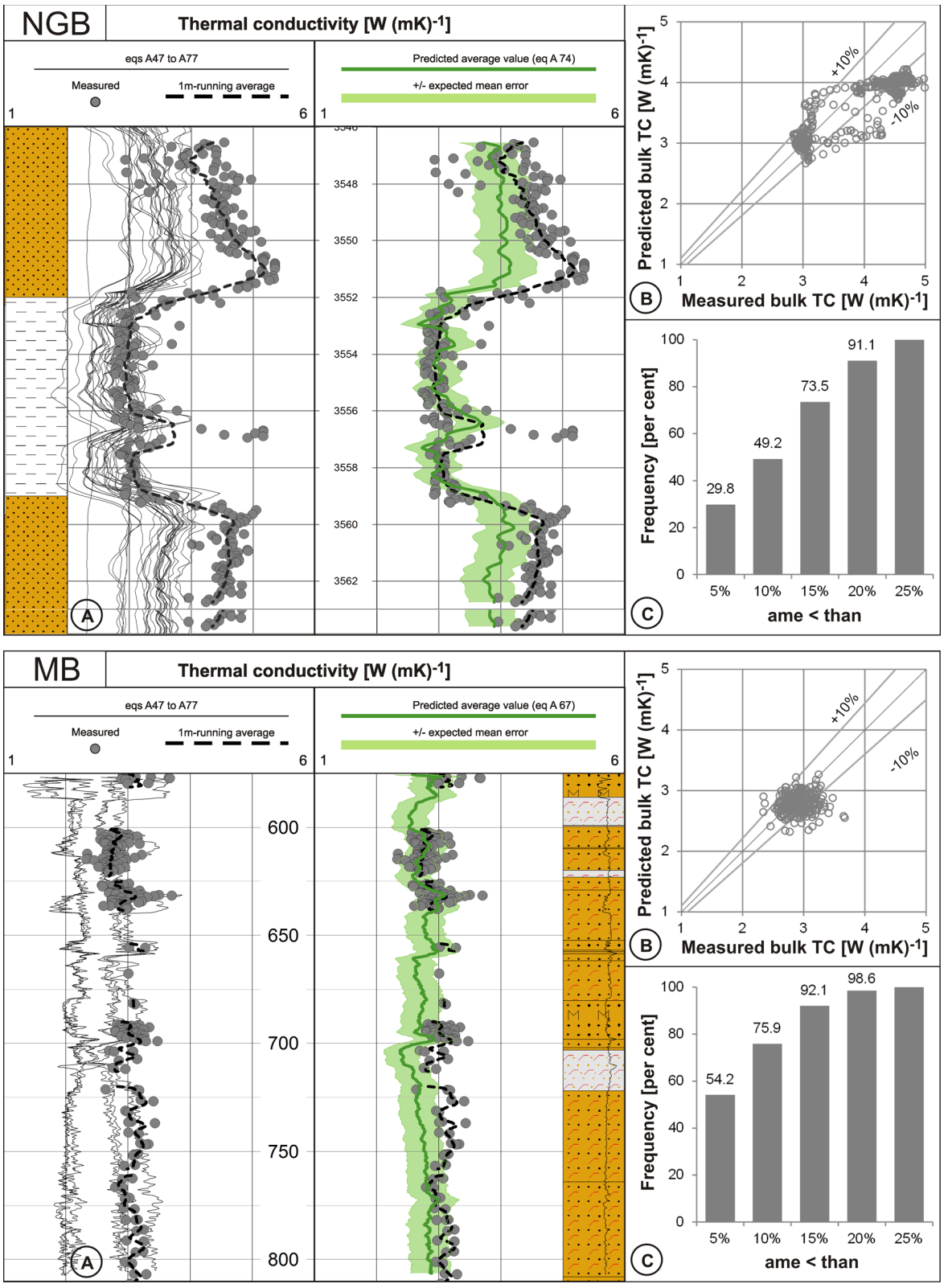

Figure 3. Validation example for the NGB (upper panel, Detfurth Formation, Middle Buntsandstein, Hannover location) and for the MB (lower panel, Tertiary, Bad-Wurzbach location). (a) Predicted TC profiles (black: individual predictions by applying different equations; dark green: average predicted value for selected equations, light green: expected mean error range) versus measured TC profiles (dark grey circles: measuring points, dashed thick black line: 1m-running average of measured data). (b) Scatter plot of predicted versus measured TC. (c) Histogram showing the distribution of the ame between measured and predicted bulk TC.

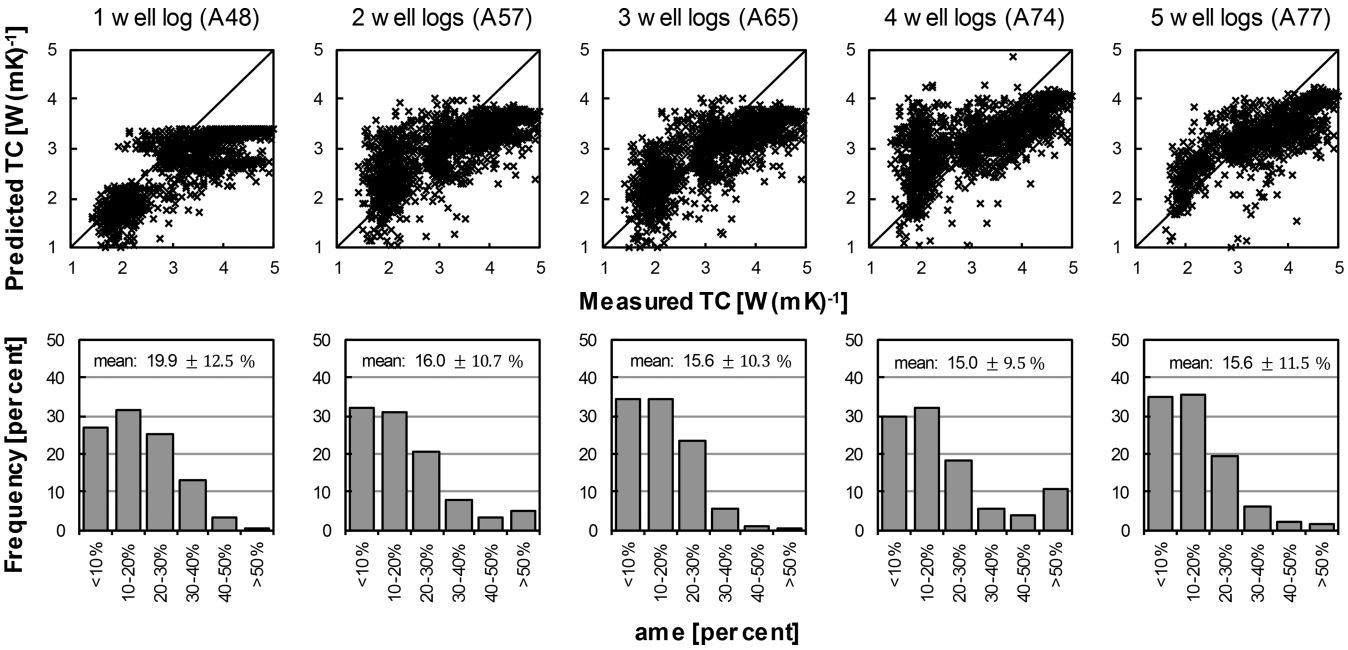

Figure 4. Scatter plot and histograms of the deviations between measured and predicted TC for the best well log combination for each number of well logs (1–5).

Appendix A. Scatter plot and histogram of the lowest deviations (best equation) between measured and predicted values are given for each number of well logs (min: 1; max: 5) for the whole data set in Fig. 4.

A detailed overview of the deviations is listed in the electronic supplementary material Table T1 for the complete data set as well as for the single formations. When comparing these deviations with those calculated from application to the test set (synthetic data set, Section 4), small differences can be observed. The averaged mean prediction deviation for all clastic equations calculated is 5.2 per cent points higher for the subsurface data set (*ca*. 18.4 per cent) than for the test set of the synthetic data set (∼13.6 per cent). While the test-set mean errors are found by the statistical methods applied to deduce the prediction equations and by the assumptions made during the method development, the slightly larger subsurface-set mean deviations cover additional uncertainties originating from the well-log measurement and the interpretation processes. Consequently, errors calculated from the test data set can be considered as a minimum prediction uncertainty (lower error limit), whereas subsurface-set mean deviations may be assumed to be close to the upper limit for real applications.

However, mean deviations reported in this chapter are calculated based on the absolute deviations, which, as a very conservative assumption, reflect TC predictions that are either always too high or too low compared to the measured TC. Considering that prediction errors of TC most likely are more or less randomly too high or too low, TC predicted along a borehole profile (e.g. for specific geological units) is expected to result in values of generally significantly lower uncertainty (Fig. 3). The mean formation TC, calculated from the predicted values, is 3.4 ± 0.4 W (m K)$^{-1}$ [Middle Buntsandstein, the NGB example] and 2.9 ± 0.2 [Süßwassermolasse, the MB example] compared with 3.7 ± 0.6 W (m K)$^{-1}$ and 2.9 ± 0.2 W (m K)$^{-1}$ for the measured values, respectively. The difference between predicted and measured formation TC amounts to 7.9 and 2.5 per cent and therewith is lower than those indicated by the equations mean deviations (9.6 and 5.8 per cent) reported above. This scale-dependent reduction of the TC variability has to be taken into account when estimating the resulting uncertainties of interval heat-flow-density values.

Previous studies on the prediction of TC (e.g. Goss & Combs 1976; Evans 1977; Molnar & Hodge 1982; Blackwell & Steele 1989; Hartmann *et al.* 2005) emphasized that empirical equations for the calculation of TC are valid only for the geological formations/materials for which they were determined. Equations developed in this study (listed in Appendix A) are deduced from a synthetic data set, and seem to be unaffected by this limitation and therefore valid for all the analysed formations and thus a broad range of continental sedimentary basins. Based on the validation of the predictions on the comprehensive database presented, we assume that the presented equations can be applied successfully also for any other clastic rocks in continental sedimentary basins. Additional data are needed to further validate the prediction equations for carbonate and evaporite rocks (Appendices B and C).

5.2 Measured versus predicted temperature profiles

Modelling of the subsurface temperature field is performed by applying a solution to the heat equation (eq. 3) with prescribed values of heat flow, TC and RHP. Thus, the quality of predicted TC values can be tested by analysing the fit of temperatures modelled with eq. (5) to high-quality borehole temperature logs.

All temperature logs used in this study were measured with a maximum sample interval of 0.1 m with logging systems having a precision generally better than 0.01 K. The temperature profiles were logged at least 1 yr after borehole completion and thus regarded as representing borehole thermal equilibrium with temperatures and temperature gradients not significantly affected by the mud circulation during the drilling process.

Temperature profiles are calculated from temperature-gradient profiles computed on the basis of a site-specific heat-flow profile and predicted *in situ* bulk TC using eq. 5. This computation was performed for borehole sections of 3.9 km length at the Hannover site (NGB) and of 2.4 km length at the Aars site (DB). Site specific heat-flow values applied in this study are: 79 mW m^{-2} (Hannover

Table 5. Comparison of logged and computed temperatures obtained using predicted bulk TC profiles for two boreholes (Groß Buchholz, NGB and Aars 1, DB).

				Logged *T*			Predicted *T*		Error	
Well	Top (m)	Bottom (m)	Length (m)	Top (°C)	Bottom (°C)	Δ (°C)	Top (°C)	Δ (°C)	Interval (per cent)	Total (°C km^{-1})
Groß Buchholz GT 1	1000	3874	2874	61.6	168.2	106.6	61.0	–0.6	0.6	0.2
Aars 1	1000	3185	2185	29.4	105.7	76.3	32.0	–2.6	3.4	1.2
	Total length:		5059 m					**Mean:**	**1.8 per cent**	**0.6 °C km^{-1}**

Note: Predicted temperature is modelled from bottom upwards. $\Delta_{\text{predicted T}}$ is the difference between the top-logged and top-predicted temperature value. The interval error is calculated as quotient of $\Delta_{\text{predicted T}}$ and Δlogged T. The total error is calculated as quotient of $\Delta_{\text{predicted T}}$ and the total length of borehole section.

location at 3800 m depth; Orilski *et al.* 2010) and 74 mW m^{-2} (Aars location at 2400 m depth; Balling 1992). Starting from these reference points, heat-flow profiles are calculated considering the RHP of the sedimentary succession by applying the relation reported in Bücker & Rybach (1996). Thus, the heat flow used for the temperature modelling ranges between 79 and 84.8 mW m^{-2} (Hannover) and between 72.9 and 75.2 mW m^{-2} (Aars). Calculation of the bulk TC profiles along continuous borehole sections demands a differentiation between different types of sedimentary rocks into evaporites, carbonate and clastic rocks. This is made using standard lithology mapping techniques (e.g. Asquith & Gibson 1982; Serra 1984) combining information from well logs and lithological descriptions from the mud reports. Then, bulk TC is calculated section-wise based on the prediction equation (listed in Appendix A) with the smallest indicated error for both the sedimentary rock group and the specific log combination in each section. Finally, a complete bulk TC profile is merged from all section-wise calculated TC profiles (44 sections for Hannover and 3 sections for Aars, Fig. 5). Accordingly, the mean prediction error to be expected along the borehole profile varies depending on the number of sections for which different predictive equations were applied. Predicted TC values were corrected to *in situ* values by applying empirical equations considering pressure (Fuchs & Förster 2014) and temperature (Somerton 1992; Zoth & Haenel 1988 where rock salt occurs).

The predicted temperature-gradient profiles, shown in Fig. 5 for the example of the NGB (Hannover) and the DB (Aars), fully reflect the changes in lithology along the borehole. Overall, approximately 80 per cent of the temperature gradients at both locations show absolute errors <10 °C km^{-1}. The largest differences are observed between 1290 and 1370 m (Lower Cretaceous) and between 1635 and 1765 m (Middle Jurassic) for the Hannover location and between 1800 and 2130 m (Lower Cretaceous) and between 2620 and 2950 m depth (Lower Jurassic) for the Aars location. On average (median), these differences between measured and modelled temperature gradients are <5 °C km^{-1}. Maximum differences in temperature gradients seem to occur particularly in layers of low porosity clay-rich units, where anisotropy in TC likely exists. This effect is difficult to quantify by any indirect method and further work is needed.

For both sites, the maximum difference in absolute temperature (modelled versus measured, Fig. 5) along the borehole profiles is <3 °C. If a fixed bottom temperature value is considered the difference between modelled and measured temperature below 1000 m depth is 0.58 per cent (Hannover location) and 3.44 per cent (Aars location; Table 5), respectively. Such a match in temperature is fully acceptable (average difference: 1.8 per cent) and meets the criteria suggested by Fuchs & Förster (2014) that an acceptable uncertainty for a modelled temperature profile would be on the order of 5–10 per cent. Ignoring the influence of temperature and pressure on the *in situ* TC would increase the absolute error to 8.2 (Hannover) and 5.4 per cent (Aars; average: 7.0 per cent).

5.3 Calculated versus predicted bulk density

Due to a general lack of measured TD and SHC data, it is hardly possible to directly validate the new well-log based prediction equations (Appendices B and C). This problem is circumnavigated by using an indirect validation approach. Based on eq. (1), only those prediction equations for TC, TD, and SHC were used in which density is not an input variable. This means that predicted bulk-density profiles are completely independent of the logged density profiles. The average uncertainty of the individual predictions for TC and SHC are used to quantify the propagation of uncertainty for the calculated bulk density. A sufficient validation of the selected TD and the SHC equations is fulfilled if the measured bulk density (log values) is within the range of calculated bulk density plus/minus the quantified propagation of uncertainty. For the Hannover example (Fig. 6), the stepwise calculation of TC, TD and SHC was performed consistently using the same well-log combination within each section. Thereby, effects that can occur by using equations based on different log combinations, and thus of varying prediction quality, are avoided. The calculated profiles of TC, TD and SHC mirror the changes in lithology quite well. Predicted bulk density is for 92 per cent of data within the expected range of values. However, further validation based on laboratory measured SHC and TD data is required to confirm the results of this indirect validation approach.

6 DISCUSSION AND APPLICATIONS

Development and application of the presented prediction equations for TC, TD and SHC are associated with a number of uncertainties. The applied ‘multimineral approach’ is based on three general assumptions: (1) that the global compositional variability in sedimentary rocks deposited in continental basins is adequately displayed by the 15 major rock-forming minerals and their range defined in Table 2; (2) that well-log response equations, mixing models (Section 2.2), and well-log-response values (Table 1) are sufficiently known to explain the ‘true’ values and (3) that multiple regression techniques are suitable for the exploration of the interrelations between parameters. Furthermore, when applying the prediction equations, accuracy depends on the uncertainties associated to the applied statistical equation, the technical quality of the well logs and the quality of the well-log interpretation itself. In most cases, users have little influence on

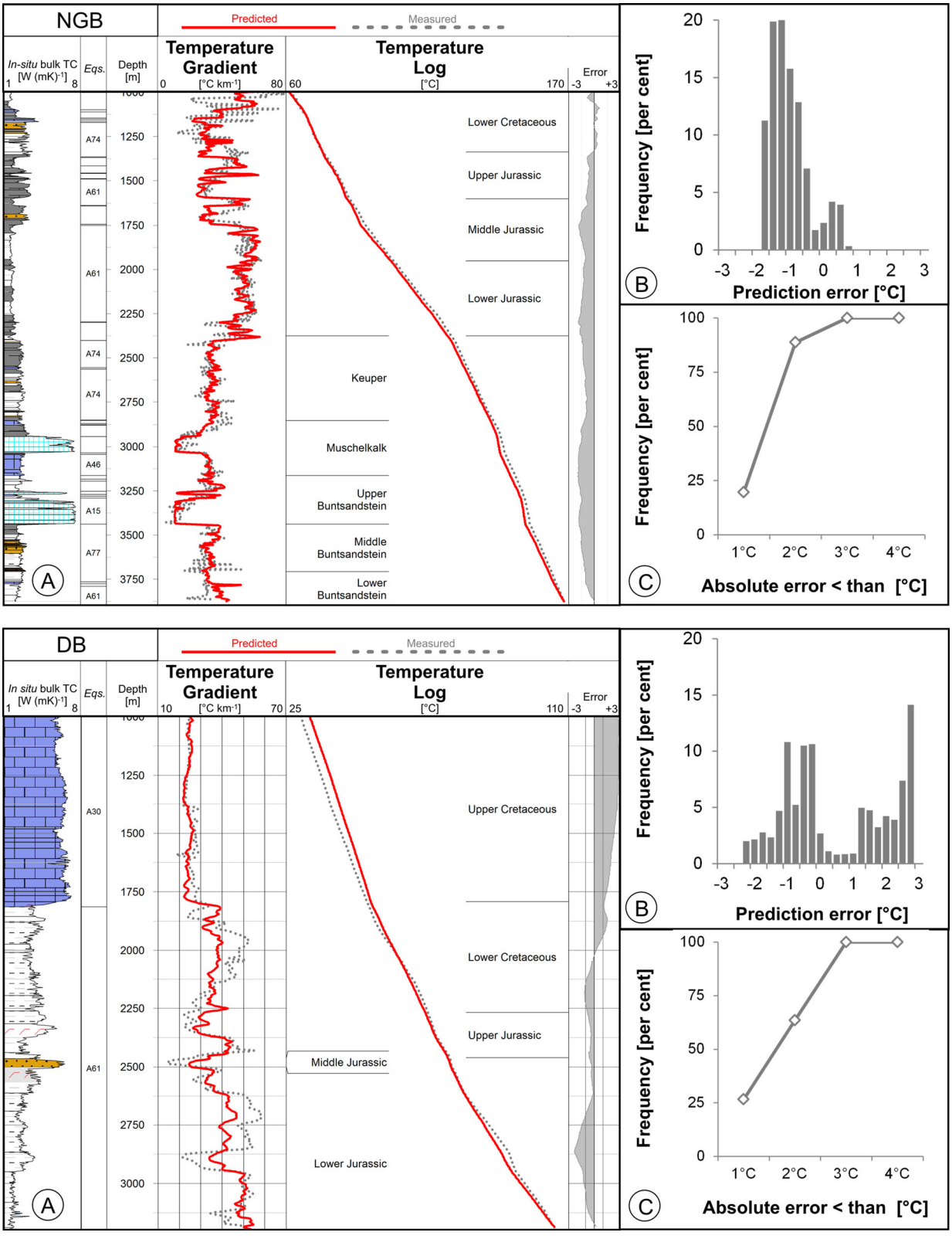

Figure 5. (a) Comparison of measured and predicted temperature and temperature gradients. Lithological descriptions are from combined analysis of drill cores, cuttings and well-log interpretation. Equations are selected regarding to the major sedimentary rock group and the available well logs. (b) Histograms showing the temperature-prediction errors as deviations between measured and predicted temperatures along the borehole. (c) Absolute error in temperature prediction accumulated along the borehole profile.

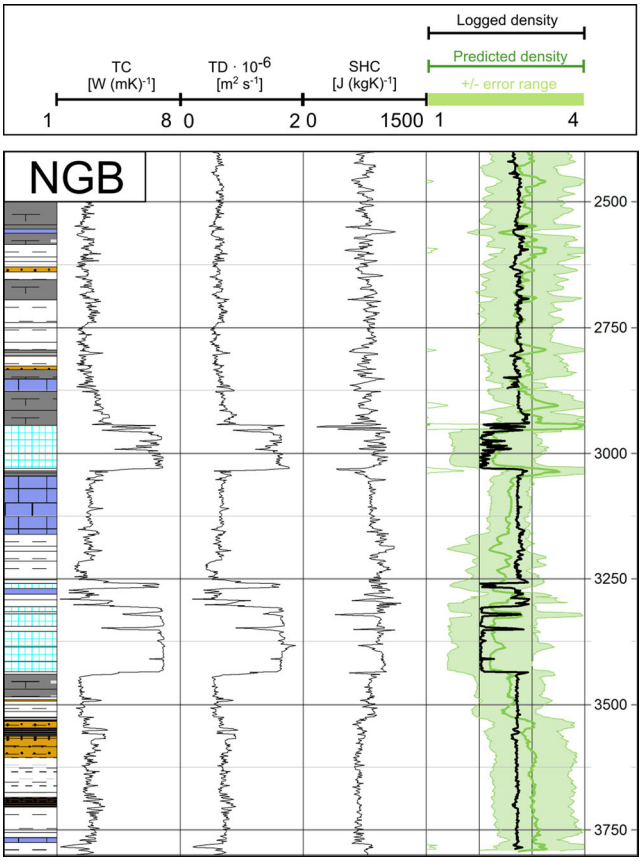

Figure 6. Validation of the well-logged based predictions of TC, TD and SHC by comparing logged bulk density with bulk density calculated following eq. (1). Examples shown are from the NGB (Hannover location).

other sources of uncertainty than the well-log interpretation. Regarding the prediction equations developed here, the quality of the following logging responses is important: neutron index, bulk density, sonic interval transit time, photoelectric factor log (for calculation of photoelectric absorption index U) and gamma ray (for V_{sh} calculation). As V_{sh} can be calculated from different sources, a spontaneous potential log has to be considered also, especially for older boreholes.

The accuracy of the predicted thermal parameters varies considerably for each parameter, the available log combination including the significance of the different logs as well as for the specific sedimentary rock group. Log readings should be correctly calibrated and rectified from environmental effects (e.g. logging speed and borehole effects, such as mud type, borehole diameter, tool positioning, mud cake and casing) to reduce uncertainties. Large impacts are known; for example, for the borehole size (borehole breakouts) on the sonic log. As the V_{sh} has a large impact in many of the proposed prediction equations, its determination should be done carefully.

Furthermore, some of the petrophysical properties are sensitive to pressure and temperature (e.g. sonic log, hydrogen index), while others are only minor affected (e.g. density log) or not affected at all (e.g. gamma ray). This is relevant for the comparison of thermal properties at ambient and *in situ* conditions, whereby the latter is most important for our purpose. For the gamma ray, no temperature-pressure effect on the log reading is to be expected because this log depends on the statistically random, spontaneous decay of atoms. Thus, the resulting thermal-property predictions are unaffected by any temperature and pressure-induced change in the log reading with depth (basic mineral values for statistical analysis are values under ambient conditions, *cf*. Section 3). Both sonic log and hydrogen index parameters show an increase with increasing pressure and a decrease with increasing temperature. Thus, a part of the temperature/pressure dependence of TC (vice versa of SHC and thus of TD as well) is probably already considered in the log reading of DT and NPHI. Post-processing of the predicted thermal-property values with an additional, empirically based in-situ correction might here result in an over correction (case: TC) or under correction (case: SHC). However, further studies on this problem are needed before a general *in-situ* correction procedure is available for the simultaneous temperature and pressure dependence of TC, SHC and TD.

6.1 Comparison with previously published equations

Fuchs & Förster (2014) discussed a large number of studies known from the literature of the past nine decades dealing with well-log based TC prediction equations. For a most promising subset of these equations, they evaluated the applicability and the prediction quality and compared them with the results of their newly developed matrix TC prediction equations. They obtained an average prediction error (ame: 16 ± 15 per cent) for the matrix TC equations, which is in fact slightly higher than for an applied benchmark equation (statistical best fit on the subsurface data set, ame: 11 ± 10 per cent), but considerably lower than for any previously published and tested equation (ame mainly between 20 and 30 per cent, some higher, up to 50 per cent). For the first time, it was demonstrated on a comprehensive data set that empirical equations developed on a synthetic data set are superior in terms of applicability to those developed on the basis of rock sample collections. In general, equations that are deduced for specific rock collections always represent a statistical optimum for this specific data set. Sometimes, perhaps as a coincidence, they show also good results for other data sets, which may be similar to the tested one.

We consider the use of large synthetic data sets for the equation development as a superior procedure to achieve a reliable TC prediction for a wide range of sedimentary rocks. Therefore, prediction quality is compared with the prediction quality of Fuchs & Förster (2014). Additionally, an inverse method is applied, which derives the major lithology of rocks from well logs (Savre 1963; Doveton & Cable 1979; Quirein *et al.* 1986). A four-component model is computed which considers the volume fractions of sandstone, shale, carbonate and porosity. By applying the geometric-mean model (eq. 10), bulk TC is then calculated for the respective lithotypes using textbook TC values (e.g. Merkel *et al.* 1976; Dove & Williams 1989; Brigaud *et al.* 1990; Demongodin, *et al.* 1991; Vasseur *et al.* 1995; Midttømme *et al.* 1997; Hartmann *et al.* 2005). The geometric-mean model is also used to calculate bulk TC from porosity and matrix TC, the latter derived from equations published by Fuchs & Förster (2014). Deviations are quantified as a 'prediction error'.

The overall mean error (18.2 ± 4.1 per cent; median of all mean errors of eqs A47–A77) to be expected in the application of bulk TC equations to clastic rocks is insignificantly higher (paired t-test, $p > 0.9$, $n = 31$) than for the matrix TC equations (17.8 ± 6.2 per cent) (*cf.* Fig. 7). The puzzling influence of porosity on the interrelations of TC with logged petrophysical properties, and thus on the deduced equations, noticed by Fuchs & Förster (2014), cannot be observed in our evaluation. The average error of the bulk TC equations shows a smaller variability than that for the matrix TC equations. As can

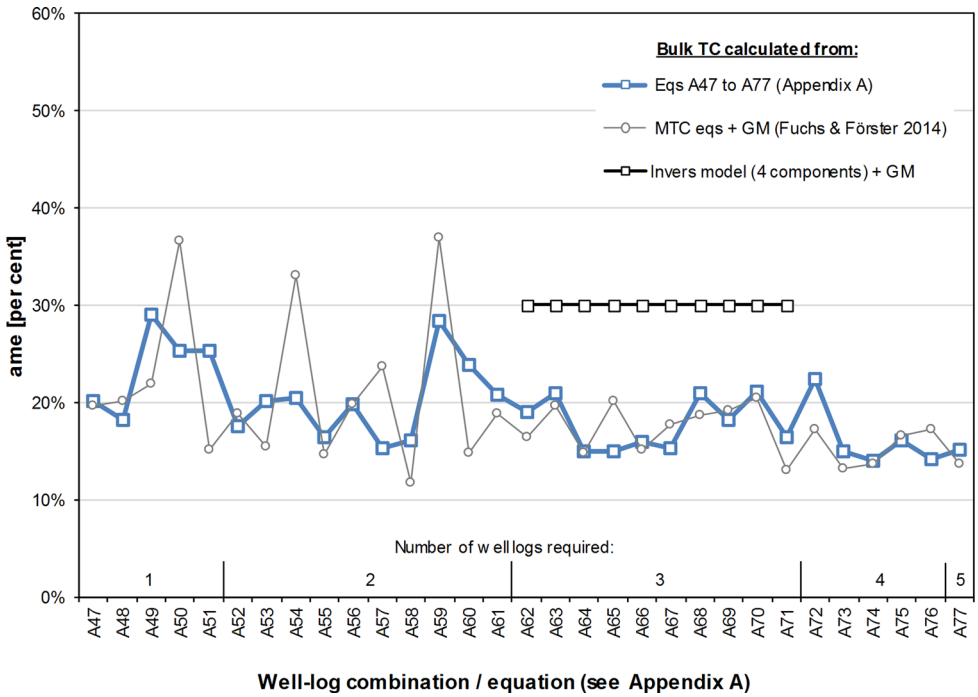

Figure 7. Average prediction errors for different well-log combinations compared on the subsurface data set of this study for the application of the new prediction equations (Appendix A), for the approach of Fuchs and Förster (2014) and for the inverse modelling (*cf.* Section 6.2).

be seen from Fig. 7, both approaches are superior to the four-component inverse prediction approach (30.1 ± 11.8 per cent). As the new prediction equations show comparable results to the approach of Fuchs & Förster (2014), it can be fairly assumed that they also excel in quality previously published empirical prediction equations evaluated in Fuchs & Förster (2014).

6.2 Palaeoclimatic impact obtained from well-log data

The well-log based prediction of TC is a valuable tool to provide data that can be used to analyze the effect of palaeoclimate upon the subsurface thermal structure, in particular in the situation of having no core and hence no TC data from laboratory measurements. A potential palaeoclimatic influence on both the shallow temperature versus depth and heat flow versus depth profiles has been known for a long time (e.g. Birch 1948; Čermák 1976; Kukkonen & Šafanda 1996). Several studies have addressed this problem specifically for the area of northern and central Europe (e.g. Clauser *et al.* 1997; Hartmann & Rath 2005; Norden *et al.* 2008; Majorowicz & Wybraniec 2010; Westaway & Younger 2013), however, no such evaluation was conducted yet for the NGB, due to the lack of reliable TC values. Knowledge about the effect of palaeoclimate is important in particular for the specification of boundary conditions (heat-flow boundary) for subsurface thermal modelling, as well as for the calibration and validation of numerical temperature models with respect to measured temperature data.

The well-log based prediction of TC demonstrated in this study allows for the first time to evaluate the palaeoclimatic impact in the NGB on the example of the Hannover site. The high-resolution temperature-log profile and the predicted TC profile (*in situ* conditions) are used to calculate temperature gradients (Fig. 8) (as described in Section 5.2) and in turn heat flow versus depth. Temperature gradients are averaged for 200-m intervals to reduce short-wave lithological impacts. Deviations between predicted and measured average temperature gradients are generally small in depth intervals below 1100 m with both positive and negative values (the average is –0.17 °C km^{-1}), whereas deviations above 1100 m are all negative and with an average of –7.32 °C km^{-1}. Heat flow calculated from the measured temperature-gradient profile and the predicted well-log based TC profile is evidently reduced in the upper part of the borehole section (Fig. 8). While heat flow below 1100 m depth averages to *ca.* 84 ± 7 mW m^{-2}, average heat flow above 700 m depth is on the order of 68 ± 7 mW m^{-2}. The extrapolated surface heat flow is *ca.* 60 mW m^{-2}, which is 25 mW m^{-2} lower than the heat-flow value from greater depth (*cf.* Section 5.2). The observed heat-flow reduction is supported by a heat-flow value of 59 mW m^{-2} reported for the Wealden Formation at approx. 1200 m depth (Orilski *et al.* 2010).

A significant overprint of the temperature by advective heat transport in Jurassic and Cretaceous aquifers can be excluded, because of the general correlation of changes in measured temperature-gradient values to lithology (and hence TC), and no sign of significant fluid flow in the temperature profile. We interpret the reduction in temperature gradients and heat flow as a clear evidence for the palaeoclimatic impact of the last glacial periods on subsurface temperatures, given the fact that heat advection in aquifers is not effective at the borehole site.

The palaeoclimatic impact quantified at the Hannover location is on the same order as theoretical models show (Norden *et al.* 2008). These models, based on palaeoclimatic data compiled by Zoth & Haenel (1988), also result in substantial temperature gradient perturbations (up to 8 °C km^{-1} compared to 10–12 °C km^{-1}, this work) from the surface down to some hundred meters. Thus it is not surprising that the location-specific terrestrial surface heat flow of 84.8 mW m^{-2} (this study) is within the range of values (68–91 mW m^{-2}) reported by Norden *et al.* (2008) as

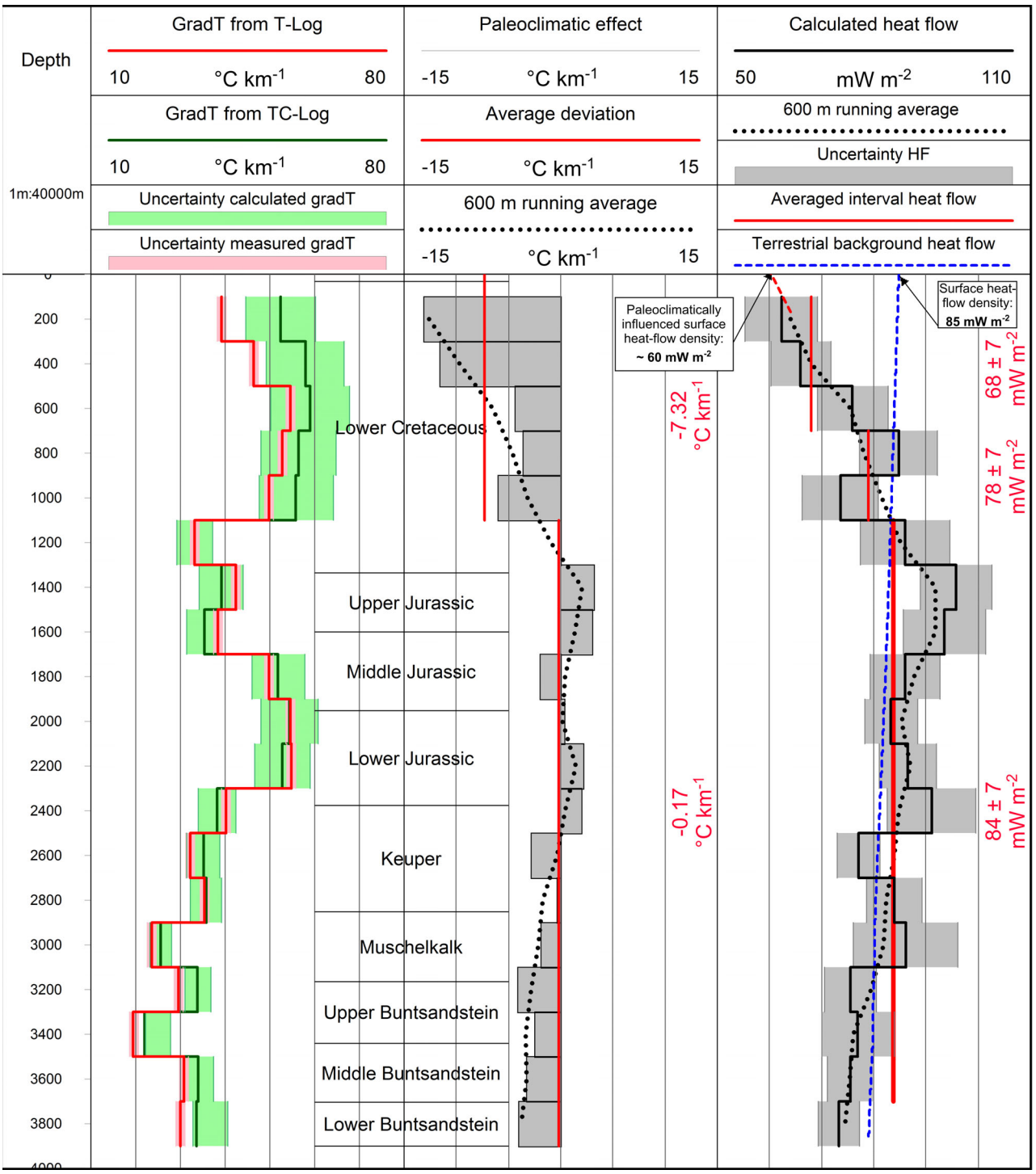

Figure 8. Estimation of the palaeoclimatic impact on the temperature-gradient profile at the Hannover location (NGB). Analysis based on the comparison of temperature gradients processed from temperature logs and temperature gradients calculated from TC profiles and given heat flow. Temperature gradients and calculated heat-flow density are shown as 200-m-mean values (grey segments) and as 600-m running average (dotted line).

palaeoclimatically undisturbed values typical for the eastern part of the NGB.

Beyond the general quantification of the palaeoclimate impact on heat flow and temperature gradients, TD profiles calculated from well logs form the basis for the study of the downward propagation of surface temperature signals and thus a direct reconstruction of the time-dependent palaeoclimatic signal. This allows determining new time-temperature series. However, this aim is clearly beyond the scope of this study.

7 CONCLUSIONS

We established new well-log based prediction equations for TC, TD and SHC of rocks in continental sedimentary basins. Presented

equations derived from a 'synthetic data set' of common sedimentary rocks describe interrelations between rock thermal properties and standard well-log data (bulk density, natural gamma-ray, sonic interval transit time, hydrogen index, photoelectric factor, and petrophysical descriptors derived from these). The presented prediction equations provide TC, TD and SHC within acceptable uncertainties. For the application of these equations to a geological site, no additional knowledge of the specific rocks types and/or their mineral composition is required. In that regard, the equations can be considered as being universally applicable.

A most obvious advantage of having calculated TC profiles at one's disposal is their use in heat-flow analysis. A comparison of modelled and measured temperature profiles and temperature gradients allows furthermore for a quantification of the palaeoclimatic effect. Those quantifications are most important for sedimentary basins in regions that have been affected by past glaciations. The study of the depth range affected by palaeoclimate perturbations and of the effects on vertical heat flow is most important for regional thermal models in which heat flow acts as a thermal boundary condition. The use of a climatically perturbed heat-flow value may significantly alter the temperature predictions made for greater depth. Thus, temperature models developed in a heat-conduction domain showing a misfit of calculated and measured temperatures at shallow depth do not necessarily point to an advective overprint on temperatures but mimic palaeoclimate.

The availability of entire borehole profiles of rock thermal properties allows for new databases that are otherwise not available. Thermal-conductivity profiles allow for high-resolution steady-state thermal models from which temperature models/maps can be retrieved. Those models are largely employed in academic research as well as in petroleum-system assessments. In turn, TD and SHC profiles can be implemented in studies of the transient temperature field in pure and applied geothermics (e.g. in palaeoclimate research and in the lifetime analysis of geothermal installations).

ACKNOWLEDGEMENTS

We are grateful to Ben Norden (GFZ, Potsdam, Germany) and Thomas Wonik (Leibniz Institute for Applied Geophysics, LIAG, Hannover, Germany) for providing background data from boreholes, logging data and core material from the North German Basin. Similar data from the Molasse Basin are provided by courtesy of Christoph Clauser (RWTH, Aachen), Andreas Hartmann (Baker Hughes) and the State Office of Geology, Raw Materials and Mining (LGRB, Freiburg; AZ 4715//05_3245). Lithological and well-log data from the Danish Basin (the Aars borehole) are provided by the Geological Survey of Denmark and Greenland (GEUS). Two anonymous reviewers and the editor Jörg Renner are acknowledged for valuable comments that helped to improve this paper.

REFERENCES

Asquith, G.B. & Gibson, C.R., 1982. *Basic Well Log Analysis for Geologists,* American Association of Petroleum Geologists, Tulsa, OK.

Balling, N., 1992. Denmark, in *Geothermal atlas of Europe—Explanatory Text,* pp. 25–28, eds Hurtig, E., Čermák, V., Haenel, R. & Zui, V. Hermann Haack Verlagsgesellschaft mbH - geographisch-Kartographisch.

Birch, A.F., 1948. The effects of Pleistocene climatic variations upon geothermal gradients, *Am. J. Sci,* **246,** 729–760.

Blackwell, D.D. & Steele, J.L., 1989. Thermal conductivity of sedimentary rocks; measurement and significance, in *Thermal History of Sedimentary Basins: Methods and Case Histories,* Vol. 14, pp. 13–36, eds Naeser, N.D. & McCulloh, T.H., Springer.

Brigaud, F. & Vasseur, G., 1989. Mineralogy, porosity and fluid control on thermal conductivity of sedimentary rocks, *Int. J. Rock Mech. Min. Sci.,* **27**(2), A77.

Brigaud, F., Chapman, D.S. & Le Douaran, S., 1990. Estimating thermal conductivity in sedimentary basins using lithologic data and geophysical well logs, *AAPG Bull.,* **74**(9), 1459–1477.

Bücker, C. & Rybach, L., 1996. A simple method to determine heat production from gamma-ray logs, *Mar. Petrol. Geol,* **13,** 373–375.

Bullard, E.C. & Day, A., 1954. The flow of heat through the floor of the Atlantic Ocean, *Geophys. J. Int,* **4,** 282–292.

Čermák, V., 1976. Processing of heat flow data—thermal conductivity and temperature gradient. in *Geoelectric and Geothermal Studies: East-Central Europe, Soviet Asia: KAPG Geophysical Monograph,* pp. 53–58, ed. Ádám, A. Akademiai Kiadao.

Čermák, V. & Rybach, L., 1982. Thermal Conductivity and Specific Heat of Minerals and Rocks, in *Geophysics—Physical Properties of Rocks,* Vol. 1, pp. 305–343, eds Beblo, M., Berktold, A., Bleil, U., Gebrande, H., Grauert, B., Haack, U., Haak, V., Kern, H., Miller, H., Petersen, N., Pohl, J., Rummel, F. & Schopper, J. R., Springer.

Clauser, C. *et al.*, 1997. The thermal regime of the crystalline continental crust: implications from the KTB, *J. geophys. Res,* **102,** 18 417–18 441.

Crain, E.R., 2013. *Crain's Petrophysical Handbook, Online Shareware, Petrophysics Training and Reference Manual,* Properties of Minerals, Available at: http://www.speC2000.net, last accessed 15 April 2013.

Demongodin, L., Pinoteau, B., Vasseur, G. & Gable, R., 1991. Thermal conductivity and well logs: a case study in the Paris Basin, *Geophys. J. Int.,* **105**(3), 675–691.

Deutsch, C.V. & Journel, A.G., 1998. *Gslib: Geostatistical Software Library and User's Guide*, pp. 369, Oxford University Press.

Dortman, N.B., 1976. *Physical Properties of Rocks and Minerals (*in Russian: *Физические свойства горных пород и полезных ископаемых: петрофизика : справочник геофизика),* pp. 526, Nedra.

Dove, R.E. & Williams, C.F., 1989. Thermal conductivity estimated from elemental concentration logs, *Nucl. Geophys.,* **3**(2), 107–112.

Doveton, J.H. & Cable, H.W., 1979. Fast matrix methods for the lithological interpretation of geophysical logs, *Comput. Geol.,* **3**(–), 101–116.

Drury, M.J., 1987. Thermal diffusivity of some crystalline rocks, *Geothermics,* **16,** 105–115.

Drury, M.J., Allen, V.S. & Jessop, A.M., 1984. The measurement of thermal diffusivity of rock cores, *Tectonophysics,* **103,** 321–333.

Evans, T.R., 1977. Thermal properties of North Sea rocks, *Log Anal.,* **18**(2), 3–12.

Fertl, W.H. & Frost, E. Jr., 1980. Evaluation of shaly clastic reservoir rocks, *J. Petrol. Technol.,* **32**(9), 1641–1646.

Fourier, J.B.J., 1822. *Théorie analytique de la chaleur,* pp. 639, Chez Firmin Didot, père et fils.

Fuchs, S. & Förster, A., 2014. Well-log based prediction of thermal conductivity of sedimentary successions: a case study from the North German Basin, *Geophys. J. Int.,* **196,** 291–311.

Fuchs, S., Schütz, F., Förster, H.-J. & Förster, A., 2013. Evaluation of common mixing models for calculating bulk thermal conductivity of sedimentary rocks: correction charts and new conversion equations, *Geothermics,* **47,** 40–52.

García, A., Contreras, E. & Domínguez, B., 1991. Developments in geothermal energy in Mexico—part thirty-three. Simultaneous determination of the thermal properties of geothermal drill cores, *Heat. Recov. Syst. CHP,* **11,** 131–139.

Goss, R.D. & Combs, J., 1976. Thermal Conductivity Measurement and Prediction from Geophysical Well Log Parameters with Borehole Application, Final Report, Institute for Geosciences, University of Texas at Dallas, NSF/RA–760364, 31 pp.

Goto, S. & Matsubayashi, O., 2008. Inversion of needle-probe data for sediment thermal properties of the eastern flank of the Juan de Fuca Ridge, *J. Geophys. Res: Solid Earth,* **113,** B08105, doi:10.1029/2007JB005119.

Goto, S. & Matsubayashi, O., 2009. Relations between the thermal properties and porosity of sediments in the eastern flank of the Juan de Fuca Ridge, *Earth Planets Space,* **61,** 863–870.

Gröber, H., Erk, S. & Grigull, U., 1955. *Die Grundgesetze der Wärmeübertragung,* Springer.

Hartmann, A. & Rath, V., 2005. Uncertainties and shortcomings of ground surface temperature histories derived from inversion of temperature logs, *J. geophys. Eng,* **2,** 299.

Hartmann, A., Rath, V. & Clauser, C., 2005. Thermal conductivity from core and well log data, *Int. J. Rock Mech. Min. Sci.,* **42**(7–8), 1042–1055.

Horai, K.-I., 1971. Thermal conductivity of rock-forming minerals, *Geophys. Res. Lett.,* **76**(5), 1278–1308.

Hyndman, R.D., Davis, E.E. & Wright, J.A., 1979. The measurement of marine geothermal heat flow by a multipenetration probe with digital acoustic telemetry and in situ thermal conductivity, *Mar. geophys. Res,* **4,** 181–205.

Kukkonen, I.T. & Šafanda, J., 1996. Palaeoclimate and structure: the most important factors controlling subsurface temperatures in crystalline rocks. A case history from Outokumpu, eastern Finland, *Geophys. J. Int,* **126,** 101–112.

Lemmon, E.W., McLinden, M.O. & Friend, D.G., 2005. Thermophysical properties of fluid systems, NIST Chemistry WebBook, NIST Standard Reference Database, 20899 pp. Lichtenecker, K., 1924. Der elektrische Leitungswiderstand künstlicher und natürlicher Aggregate, *Physik Zeitschr,* **25**(8), 169–181, 193–204, 226–233.

Lichtenecker, K., 1924. Der elektrische Leitungswiderstand künstlicher und natürlicher Aggregate, *Physik. Zeitschr,* **25,** 169–181, 193–204, 226–233.

Majorowicz, J.A. & Wybraniec, S., 2010. New terrestrial heat flow map of Europe after regional palaeoclimatic correction application, *Int. J. Earth. Sci.,* 1–7.

Mel'nikova, N.V., Rzhevskogo, V.V. & Protod'yakonova, M.M., 1975. *Spravochnik (Kadastr) Fisicheskikh Svoystv Gornykh Porod (in English: Handbook [Registry] of Physical Properties of Rocks),* pp. 279, Nedra.

Merkel, R.H., Maccary, L.M. & Chico, R.S., 1976. Computer techniques applied to formation evaluation, *Log Anal.,* **17**(3), 3–10.

Midttømme, K., Roaldset, E. & Aagaard, P., 1997. Thermal conductivity of argillaceous sediments, in *Modern Geophysics in Engineering Geology,* Vol. 12, pp. 355–363, eds McCann, D. M., Eddleston, M., Fenning, P. J. & Reeves, G.M., Geological Society Engineering Geology.

Molnar, P.S. & Hodge, D., 1982. Correlation of thermal conductivity with physical properties obtained from geophysical well logs, in *Proceedings of the AAPG Annual Convention with Divisions SEPM/EMD/DPA,* June 27–30, 1982, Calgary, AB, Canada, pp. 608–609.

Norden, B., Förster, A. & Balling, N., 2008. Heat flow and lithospheric thermal regime in the Northeast German Basin, *Tectonophysics,* **460,** 215–229.

Orilski, J., Schellschmidt, R. & Wonik, T., 2010. Temperaturverlauf und Wärmeleitfähigkeit im Untergrund der Bohrung Groß Buchholz GT1 in Hannover, in *Proceedings of the Geothermiekongress 2010, 17.-19. November 2010,* Karlsruhe, 10 pp.

Quirein, J., Kimminau, S., La Vigne, J., Singer, J. & Wendel, F., 1986. A coherent framework for developing and applying multiple formation evaluation models, in *Proceedings of the SPWLA 27th Annual Logging Symposium,* Houston. June 9–13, 17 pp.

Reuss, A., 1929. Berechnung der Fließgrenze von Mischkristallen auf Grund der Plastizitätsbedingung für Einkristalle, *Z. angew. Math. Mech,* **9,** 49–58.

Richardson, M.J., 1993. The specific heats of coals, cokes and their ashes, *Fuel,* **72,** 1047–1053.

Rybach, L., 1986. Amount and significance of radioactive heat sources in sediments, in *Thermal Modelling in Sedimentary Basins: 1st IFP Exploration Research Conference Carcans,* pp. 311–322, ed. Burrus, J. Editions Technip, Carcans.

Savre, W.C., 1963. Determination of a more accurate porosity and mineral composition in complex lithologies with the use of the sonic, neutron and density Surveys, *J. Petrol. Technol.,* **15**(9), 945–959.

Schön, J., 1983. *Petrophysik. Physikalische Eigenschaften von Gesteinen und Mineralien,* Enke Ferdinand.

Schön, J.-H., 1996. Physical Properties of Rocks, Fundamentals and Principles of Petrophysics, in *Handbook of Geophysical Exploration: Seismic Exploration* Vol. 18, pp. 583, eds Helbig, K. & Treitel, S., Pergamon.

Serra, O., 1984. *Fundamentals of Well-Log Interpretation—The Acquisition of Logging Data,* Elsevier.

Skauge, A., Fuller, N. & Hepler, L.G., 1983. Specific heats of clay minerals: Sodium and calcium kaolinites, sodium and calcium montmorillonites, illite, and attapulgite, *Thermochim. Acta,* **61,** 139–145.

Somerton, W.H., 1992. *Thermal Properties and Temperature-Related Behavior of Rock/Fluid Systems,* Elsevier Science Publishers.

van Krevelen, D.W., 1961. *Coal: Typology, Chemistry, Physics, Constitution,* 2 edn, pp. 514, Elsevier Publishing Company.

Vasseur, G., Brigaud, F. & Demongodin, L., 1995. Thermal conductivity estimation in sedimentary basins, *Tectonophysics,* **244**(1–3), 167–174.

Voigt, W., 1928. *Lehrbuch der Kristallphysik,* pp. 978, Teubner.

Von Herzen, R. & Maxwell, A.E., 1959. The measurement of thermal conductivity of deep-sea sediments by a needle-probe method, *J. geophys. Res.,* **64**(10), 1557–1563.

Waples, D.W. & Waples, J.S., 2004. A review and evaluation of specific heat capacities of rocks, minerals, and subsurface fluids. Part 2: fluids and porous rocks, *Nat. Resour. Res,* **13,** 123–130.

Westaway, R. & Younger, P.L., 2013. Accounting for palaeoclimate and topography: a rigorous approach to correction of the British geothermal dataset, *Geothermics,* **48,** 31–51.

Ziegler, P.A., 1990. *Geological Atlas of Western and Central Europe*, ed. Ziegler, P. A., The Hague (Shell).

Zoth, G. & Haenel, R., 1988. Appendix. in *Handbook of Terrestrial Heat-Flow Density Determination*, pp. 449–468, eds Haenel, R., Rybach, L. & Stegena, L., Kluwer Academic Publishers.

SUPPORTING INFORMATION

Additional Supporting Information may be found in the online version of this paper:

Table T1. Bulk-TC equations for variable well-log combinations (T1.csv).

Table T2. Bulk-TD equations for variable well-log combinations (T2.csv).

Table T3. Bulk-SHC equations for variable well-log combinations (T3.csv).

(http://gji.oxfordjournals.org/lookup/suppl/doi:10.1093/gji/ggv403/-/DC1).

Please note: Oxford University Press is not responsible for the content or functionality of any supporting materials supplied by the authors. Any queries (other than missing material) should be directed to the corresponding author for the paper.

APPENDIX A: BULK-TC EQUATIONS FOR VARIABLE WELL-LOG COMBINATIONS

	Eq. #	No. of	Bulk-TC-prediction equations [TCB in W (mK)$^{-1}$]										R^2	Mean	SD	Rms
		logs	b_o	b_{RHOB}		b_{PHIN}		b_U		b_{DT}		b_{VSH}			[per cent]	
Evaporites (n = 286)	A1	1	5.31	–0.809	ρ_b									0.020	46.3	51.0	68.7
	A2	1	5.34			–8.14	φ_N							0.741	18.0	14.5	23.1
	A3	1	–0.93					+0.437	U					0.312	37.8	30.9	48.7
	A4	1	3.73							–0.00117	ΔT			0.002	45.8	47.8	65.9
	A5	2	10.73	–2.223	ρ_b	–9.21	φ_N							0.903	11.4	11.0	15.8
	A6	2	2.09	–1.504	ρ_b			+0.483	U					0.386	37.1	33.1	49.5
	A7	2	15.69	–3.455	ρ_b					–0.01725	ΔT			0.116	46.3	58.3	74.1
	A8	2	5.34			–8.14	φ_N	+0.000	U					0.740	18.0	14.5	23.1
	A9	2	3.46			–9.07	φ_N			+0.00847	ΔT			0.814	16.7	15.3	22.6
	A10	2	–2.25					+0.469	U	+0.00405	ΔT			0.327	37.3	29.9	47.6
	A11	3	10.52	–2.227	ρ_b	–9.07	φ_N	+0.019	U					0.903	11.6	10.8	15.8
	A12	3	14.40	–3.157	ρ_b	–8.97	φ_N			–0.00634	ΔT			0.915	11.2	9.7	14.8
	A13	3	8.50	–3.032	ρ_b			+0.450	U	–0.01028	ΔT			0.418	37.3	39.1	53.9
	A14	3	3.11			–8.86	φ_N	+0.028	U	+0.00855	ΔT			0.815	16.9	15.1	22.6
	A15	4	14.32	–3.153	ρ_b	–8.93	φ_N	+0.005	U	–0.00631	ΔT			0.915	11.2	9.8	14.8
Carbonates (n = 15,764)	A16	1	–4.45	+2.985	ρ_b									0.560	13.7	11.6	17.9
	A17	1	3.92			–5.11	φ_N							0.591	13.6	10.4	17.1
	A18	1	1.76					+0.118	U					0.065	21.1	15.2	26.0
	A19	1	5.56							–0.01200	ΔT			0.556	13.6	10.1	17.0
	A20	1	3.60									–1.96	V_{sh}	0.395	17.2	11.6	20.7
	A21	2	0.08	+1.411	ρ_b	–3.15	φ_N							0.630	12.8	10.0	16.2
	A22	2	–6.45	+4.648	ρ_b			–0.270	U					0.724	11.4	9.3	14.7
	A23	2	0.24	+1.632	ρ_b					–0.00600	ΔT			0.587	13.2	10.4	16.8
	A24	2	–2.40	+2.393	ρ_b							–1.29	V_{sh}	0.709	11.6	8.4	14.3
	A25	2	4.84			–5.88	φ_N	–0.101	U					0.625	13.1	10.8	17.0
	A26	2	4.43			–3.78	φ_N			–0.00340	ΔT			0.597	13.4	10.3	16.9
	A27	2	4.24			–4.08	φ_N					–1.17	V_{sh}	0.707	11.4	8.2	14.1
	A28	2	7.02					–0.120	U	–0.01418	ΔT			0.601	13.4	10.6	17.1
	A29	2	3.39					+0.025	U			–1.90	V_{sh}	0.397	17.0	11.7	20.6
	A30	2	5.84							–0.00997	ΔT	–1.48	V_{sh}	0.767	9.8	7.2	12.1
	A31	3	–2.80	+3.301	ρ_b	–2.43	φ_N	–0.248	U					0.764	10.6	8.5	13.6
	A32	3	–1.39	+1.763	ρ_b	–4.01	φ_N			+0.00344	ΔT			0.633	12.8	10.0	16.3
	A33	3	0.59	+1.340	ρ_b	–2.24	φ_N					–1.15	V_{sh}	0.742	10.7	7.8	13.2
	A34	3	–4.37	+4.005	ρ_b			–0.259	U	–0.00253	ΔT			0.729	11.3	9.1	14.5
	A35	3	–4.37	+4.178	ρ_b			–0.302	U			–1.45	V_{sh}	0.912	6.4	4.9	8.0
	A36	3	5.01	+0.254	ρ_b					–0.00910	ΔT	–1.45	V_{sh}	0.768	9.8	7.2	12.1
	A37	3	5.88			–3.74	φ_N	–0.119	U	–0.00582	ΔT			0.641	12.7	10.6	16.6
	A38	3	5.46			–4.97	φ_N	–0.130	U			–1.28	V_{sh}	0.762	10.7	8.0	13.4
	A39	3	6.19			+1.08	φ_N			–0.01226	ΔT	–1.58	V_{sh}	0.769	9.7	7.1	12.0
	A40	3	8.24					–0.194	U	–0.01345	ΔT	–1.74	V_{sh}	0.877	7.6	6.2	9.8
	A41	4	–6.19	+4.191	ρ_b	–4.25	φ_N	–0.264	U	+0.00749	ΔT			0.781	10.4	8.3	13.3
	A42	4	–2.67	+3.534	ρ_b	–1.21	φ_N	–0.290	U			–1.37	V_{sh}	0.921	6.0	4.6	7.6
	A43	4	5.77	+0.119	ρ_b	+1.00	φ_N			–0.01168	ΔT	–1.56	V_{sh}	0.770	9.7	7.1	12.0
	A44	4	0.33	+2.731	ρ_b			–0.280	U	–0.00559	ΔT	–1.54	V_{sh}	0.933	5.4	4.5	7.0
	A45	4	9.12			+2.36	φ_N	–0.204	U	–0.01863	ΔT	–1.97	V_{sh}	0.888	7.2	5.8	9.3
	A46	5	1.15	+2.587	ρ_b	+1.08	φ_N	–0.280	U	–0.00838	ΔT	–1.66	V_{sh}	0.935	5.2	4.6	6.9

(*Continued.*)

	Eq. #	No. of	Bulk-TC-prediction equations [TCB in W (mK)$^{-1}$]										R^2	Mean	SD	Rms
		logs	b_o	b_{RHOB}		b_{PHIN}		b_U		b_{DT}		b_{VSH}			[per cent]	
Clastic rocks (n = 151,021)	A47	1	–3.30	+2.361	ρ_b									0.364	17.6	13.2	22.0
	A48	1	3.41			–4.83	φ_N							0.511	15.4	11.2	19.0
	A49	1	2.14					+0.029	U					0.004	23.0	16.2	28.1
	A50	1	4.81							–0.00974	ΔT			0.376	17.5	12.0	21.2
	A51	1	3.60									–2.31	V_{sh}	0.455	17.0	12.5	21.1
	A52	2	2.52	+0.331	ρ_b	–4.38	φ_N							0.513	15.3	11.2	18.9
	A53	2	–5.70	+4.364	ρ_b			–0.335	U					0.628	13.7	10.6	17.3
	A54	2	1.14	+1.117	ρ_b					–0.00578	ΔT			0.396	17.2	12.2	21.0
	A55	2	–1.28	+1.974	ρ_b							–2.02	V_{sh}	0.703	12.6	9.7	15.9
	A56	2	4.03			–5.17	φ_N	–0.077	U					0.536	15.1	11.5	19.0
	A57	2	1.01			–10.87	φ_N			+0.01474	ΔT			0.578	14.4	11.1	18.2
	A58	2	4.17			–3.89	φ_N					–1.78	V_{sh}	0.762	11.0	8.8	14.1
	A59	2	6.20					–0.126	U	–0.01170	ΔT			0.435	16.7	12.4	20.7
	A60	2	2.90					+0.115	U			–2.52	V_{sh}	0.513	15.9	11.8	19.8
	A61	2	5.59							–0.00840	ΔT	–2.05	V_{sh}	0.730	11.7	9.3	15.0
	A62	3	–3.87	+3.577	ρ_b	–1.15	φ_N	–0.293	U					0.634	13.5	10.4	17.1
	A63	3	–6.93	+2.226	ρ_b	–12.64	φ_N			+0.02662	ΔT			0.650	13.0	10.3	16.6
	A64	3	2.54	+0.609	ρ_b	–3.03	φ_N					–1.81	V_{sh}	0.771	10.8	8.6	13.8
	A65	3	0.94			–10.95	φ_N	+0.003	U	+0.01498	ΔT			0.578	14.4	11.1	18.1
	A66	3	4.08			–3.82	φ_N	+0.013	U			–1.81	V_{sh}	0.763	11.0	8.7	14.0
	A67	3	3.66			–5.13	φ_N			+0.00293	ΔT	–1.70	V_{sh}	0.764	11.0	8.7	14.0
	A68	3	5.76					–0.018	U	–0.00870	ΔT	–2.01	V_{sh}	0.731	11.7	9.3	15.0
	A69	3	3.34	+0.681	ρ_b					–0.00600	ΔT	–2.03	V_{sh}	0.737	11.6	9.2	14.8
	A70	3	–7.95	+5.097	ρ_b			–0.360	U	+0.00270	ΔT			0.633	13.7	10.6	17.3
	A71	3	–3.14	+3.187	ρ_b			–0.186	U			–1.49	V_{sh}	0.761	11.2	9.0	14.3
	A72	4	–10.01	+4.361	ρ_b	–8.55	φ_N	–0.226	U	+0.02145	ΔT			0.717	12.0	9.5	15.3
	A73	4	0.36	+1.685	ρ_b	–2.09	φ_N	–0.100	U			–1.59	V_{sh}	0.781	10.6	8.6	13.6
	A74	4	–1.55	+1.386	ρ_b	–6.81	φ_N			+0.01152	ΔT	–1.53	V_{sh}	0.790	10.4	8.1	13.2
	A75	4	–1.06	+2.491	ρ_b			–0.155	U	–0.00230	ΔT	–1.58	V_{sh}	0.765	11.0	8.9	14.2
	A76	4	2.94			–6.00	φ_N	+0.038	U	+0.00551	ΔT	–1.73	V_{sh}	0.768	10.8	8.5	13.8
	A77	5	–3.60	+2.416	ρ_b	–5.84	φ_N	–0.097	U	+0.01133	ΔT	–1.32	V_{sh}	0.800	10.2	8.1	13.0

Note: Equations are formulated with unstandardized regression coefficients. R^2 is calculated on the synthetic regression set; mean, sd, and rms are calculated on the synthetic testing set. Reduced number of equations for evaporites is induced by non-correlation of VSH to the set of evaporites. For abbreviations see the Appendix D. Multiple regression equations are basically read as: $\alpha = b_0 + b_{RHOB} \cdot RHOB + b_{PHIN} \cdot PHIN + b_U \cdot \underline{U} + b_{DT} \cdot DT + b_{VSH} \cdot VSH$. B_x are unstandardized regression coefficients listed in the appendix, greek letters are well-log values. Where a specific regression coefficient is not noted, the associated well-log type is not included in the regression.

APPENDIX B: BULK-TD EQUATIONS FOR VARIABLE WELL-LOG COMBINATIONS

	Eq. #	No. of logs	Bulk-TD-prediction equations [TD in 10^{-6} m^2 s^{-1}]										R^2	Mean	SD	Rms
			b_o	b_{RHOB}		b_{PHIN}		b_U		b_{DT}		b_{VSH}			[per cent]	
Evaporites (n = 286)	B1	1	2.09	−0.27	ρ_b									0.005	61.9	68.5	92.0
	B2	1	2.49			−4.35	φ_N							0.728	25.2	27.9	37.5
	B3	1	−1.25					+0.27	U					0.417	42.6	33.5	54.0
	B4	1	1.91							−0.00180	ΔT			0.009	60.7	63.0	87.2
	B5	2	4.94	−1.01	ρ_b	−4.84	φ_N							0.843	21.8	23.5	31.9
	B6	2	0.14	−0.69	ρ_b			+0.29	U					0.470	43.1	36.0	56.0
	B7	2	8.50	−1.90	ρ_b					−0.01065	ΔT			0.132	60.5	79.3	99.2
	B8	2	1.70			−3.83	φ_N	+0.07	U					0.742	25.3	26.8	36.7
	B9	2	1.78			−4.71	φ_N			+0.00321	ΔT			0.764	26.8	28.9	39.3
	B10	2	−1.69					+0.28	U	+0.00135	ΔT			0.421	42.3	32.9	53.5
	B11	3	4.10	−1.03	ρ_b	−4.26	φ_N	+0.07	U					0.861	20.8	22.4	30.4
	B12	3	7.83	−1.75	ρ_b	−4.65	φ_N			−0.00499	ΔT			0.870	19.6	19.5	27.6
	B13	3	4.14	−1.65	ρ_b			+0.27	U	−0.00642	ΔT			0.513	43.9	45.4	63.0
	B14	3	0.80			−4.12	φ_N	+0.08	U	+0.00345	ΔT			0.783	25.6	28.0	37.8
	B15	4	6.86	−1.70	ρ_b	−4.16	φ_N	+0.06	U	−0.00457	ΔT			0.883	19.0	19.6	27.2
Carbonates (n = 15,764)	B16	1	−2.67	+1.58	ρ_b									0.614	16.1	13.3	20.9
	B17	1	1.83			−2.95	φ_N							0.769	12.4	9.2	15.5
	B18	1	0.57					+0.07	U					0.089	27.0	19.4	33.3
	B19	1	2.79							−0.00687	ΔT			0.734	12.7	9.0	15.5
	B20	1	1.45									−0.75	V_{sh}	0.226	25.8	17.3	31.0
	B21	2	0.86	+0.36	ρ_b	−2.46	φ_N							0.778	12.0	9.1	15.1
	B22	2	−3.61	+2.37	ρ_b			−0.13	U					0.757	13.1	10.3	16.7
	B23	2	2.41	+0.12	ρ_b					−0.00645	ΔT			0.735	12.7	9.1	15.6
	B24	2	−2.11	+1.42	ρ_b							−0.35	V_{sh}	0.657	15.8	11.7	19.7
	B25	2	2.34			−3.37	φ_N	−0.06	U					0.809	11.4	9.2	14.7
	B26	2	2.19			−2.01	φ_N			−0.00239	ΔT			0.780	11.8	8.7	14.6
	B27	2	1.89			−2.76	φ_N					−0.21	V_{sh}	0.784	12.1	8.9	15.1
	B28	2	3.62					−0.07	U	−0.00821	ΔT			0.790	11.6	8.4	14.3
	B29	2	1.14					+0.04	U			−0.67	V_{sh}	0.248	24.7	17.2	30.1
	B30	2	2.88							−0.00632	ΔT	−0.44	V_{sh}	0.809	10.9	7.8	13.4
	B31	3	−0.39	+1.18	ρ_b	−2.14	φ_N	−0.11	U					0.879	9.1	7.2	11.6
	B32	3	1.58	+0.18	ρ_b	−2.04	φ_N			−0.00168	ΔT			0.782	11.7	8.8	14.7
	B33	3	0.96	+0.34	ρ_b	−2.29	φ_N					−0.21	V_{sh}	0.793	11.8	8.8	14.7
	B34	3	0.53	+1.09	ρ_b			−0.11	U	−0.00505	ΔT			0.827	10.7	7.9	13.3
	B35	3	−3.00	+2.23	ρ_b			−0.14	U			−0.43	V_{sh}	0.821	11.4	8.4	14.2
	B36	3	4.01	−0.34	ρ_b					−0.00750	ΔT	−0.48	V_{sh}	0.814	10.7	7.7	13.2
	B37	3	3.01			−1.99	φ_N	−0.07	U	−0.00376	ΔT			0.835	10.5	8.1	13.3
	B38	3	2.47			−3.18	φ_N	−0.06	U			−0.27	V_{sh}	0.832	11.1	8.6	14.0
	B39	3	2.59			−0.90	φ_N			−0.00442	ΔT	−0.36	V_{sh}	0.816	10.8	7.8	13.3
	B40	3	4.02					−0.09	U	−0.00797	ΔT	−0.57	V_{sh}	0.906	7.9	6.9	10.5
	B41	4	−0.39	+1.18	ρ_b	−2.13	φ_N	−0.11	U	−0.00002	ΔT			0.879	9.1	7.2	11.6
	B42	4	−0.37	+1.23	ρ_b	−1.87	φ_N	−0.12	U			−0.30	V_{sh}	0.908	8.0	6.4	10.3
	B43	4	3.45	−0.24	ρ_b	−0.73	φ_N			−0.00561	ΔT	−0.41	V_{sh}	0.818	10.6	7.7	13.2
	B44	4	2.12	+0.65	ρ_b			−0.11	U	−0.00609	ΔT	−0.52	V_{sh}	0.919	7.1	6.4	9.6
	B45	4	3.89			−0.33	φ_N	−0.09	U	−0.00725	ΔT	−0.54	V_{sh}	0.907	7.9	6.9	10.5
	B46	5	1.59	+0.75	ρ_b	−0.70	φ_N	−0.11	U	−0.00429	ΔT	−0.45	V_{sh}	0.922	7.1	6.2	9.4

(*Continued.*)

	Eq. #	No. of logs	Bulk-TD-prediction equations [TD in 10^{-6} m^2 s^{-1}]										R^2	Mean	SD	Rms
			b_o	b_{RHOB}		b_{PHIN}		b_U		b_{DT}		b_{VSH}			[per cent]	
Clastic rocks ($n = 151{,}021$)	B47	1	−2.42	+1.44	ρ_b									0.437	21.7	17.7	28.0
	B48	1	1.69			−3.09	φ_N							0.675	15.7	11.3	19.4
	B49	1	0.84					+0.02	U					0.009	31.1	23.8	39.2
	B50	1	2.68							−0.00659	ΔT			0.559	18.2	13.3	22.6
	B51	1	1.54									−0.97	V_{sh}	0.261	27.2	20.1	33.8
	B52	2	1.66	+0.01	ρ_b	−3.07	φ_N							0.675	15.7	11.3	19.4
	B53	2	−3.79	+2.58	ρ_b			−0.19	U					0.714	15.6	12.2	19.8
	B54	2	2.43	+0.08	ρ_b					−0.00633	ΔT			0.559	18.2	13.4	22.6
	B55	2	−1.64	+1.29	ρ_b							−0.78	V_{sh}	0.602	19.2	14.7	24.2
	B56	2	2.04			−3.28	φ_N	−0.04	U					0.700	15.3	11.3	19.0
	B57	2	0.94			−4.99	φ_N			+0.00465	ΔT			0.697	15.3	11.2	19.0
	B58	2	1.95			−2.77	φ_N			−0.00783		−0.60	V_{sh}	0.766	14.0	10.9	17.7
	B59	2	3.56					−0.08	U		ΔT			0.635	16.8	12.5	20.9
	B60	2	1.17					+0.06	U	−0.00608		−1.09	V_{sh}	0.314	25.6	19.5	32.2
	B61	2	2.98								ΔT	−0.79	V_{sh}	0.727	15.2	11.9	19.3
	B62	3	−1.21	+1.48	ρ_b	−1.62	φ_N	−0.13	U	+0.00760				0.754	14.1	10.8	17.8
	B63	3	−1.03	+0.55	ρ_b	−5.43	φ_N				ΔT			0.711	15.0	11.1	18.7
	B64	3	1.67	+0.10	ρ_b	−2.63	φ_N			+0.00248		−0.60	V_{sh}	0.767	13.9	10.9	17.7
	B65	3	1.53			−4.23	φ_N	−0.03	U		ΔT			0.704	15.2	11.3	18.9
	B66	3	2.06			−2.86	φ_N	−0.02	U	+0.00064		−0.55	V_{sh}	0.769	13.9	10.9	17.6
	B67	3	1.84			−3.04	φ_N			−0.00681	ΔT	−0.58	V_{sh}	0.766	13.9	10.9	17.7
	B68	3	3.41					−0.04	U	−0.00641	ΔT	−0.69	V_{sh}	0.746	14.6	11.7	18.7
	B69	3	3.29	−0.09	ρ_b					−0.00236	ΔT	−0.79	V_{sh}	0.727	15.2	11.9	19.3
	B70	3	−1.82	+1.94	ρ_b			−0.17	U		ΔT			0.728	15.0	11.6	18.9
	B71	3	−3.21	+2.31	ρ_b			−0.16	U	+0.00493		−0.34	V_{sh}	0.737	15.2	11.9	19.4
	B72	4	−2.62	+1.65	ρ_b	−3.32	φ_N	−0.12	U		ΔT			0.768	13.8	10.4	17.3
	B73	4	−0.08	+0.97	ρ_b	−1.87	φ_N	−0.08	U	+0.00220		−0.43	V_{sh}	0.788	13.3	10.6	17.0
	B74	4	0.89	+0.25	ρ_b	−3.35	φ_N			−0.00391	ΔT	−0.55	V_{sh}	0.769	13.9	10.7	17.6
	B75	4	0.31	+1.13	ρ_b			−0.11	U	−0.00060	ΔT	−0.49	V_{sh}	0.768	14.0	11.2	17.9
	B76	4	2.18			−2.62	φ_N	−0.02	U	+0.00205	ΔT	−0.56	V_{sh}	0.769	13.9	10.9	17.7
	B77	5	−0.79	+1.10	ρ_b	−2.55	φ_N	−0.08	U	+0.01133	ΔT	−0.38	V_{sh}	0.790	13.3	10.4	16.9

Note: Equations are formulated with unstandardized regression coefficients. R^2 is calculated on the synthetic regression set; mean, sd, and rms are calculated on the synthetic testing set. Reduced number of equations for evaporites is induced by non-correlation of VSH to the set of evaporites. For abbreviations see the Appendix D. Multiple regression equations are basically read as: $\lambda = b_0 + b_{RHOB} \cdot RHOB + b_{PHIN} \cdot PHIN + b_U \cdot \underline{U} + b_{DT} \cdot DT + b_{VSH} \cdot VSH$. B_x are unstandardized regression coefficients listed in the appendix, greek letters are well log values. Where a specific regression coefficient is not noted, the associated well-log type is not included in the regression.

APPENDIX C: BULK-SHC EQUATIONS FOR VARIABLE WELL-LOG COMBINATIONS

	Eq. #	No. of logs	Bulk-SHC prediction equations [SHC in J (kgK)$^{-1}$]										R^2	Mean	SD	Rms
			b_o	b_{RHOB}		b_{PHIN}		b_U		b_{DT}		b_{VSH}		[per cent]		
Evaporites (n = 286)	C1	1	2973.7	−708.2	ρ_b									0.390	16.9	14.5	22.2
	C2	1	1012.5			+1382.1	φ_N							0.473	15.6	13.8	20.7
	C3	1	2412.5					−107.9	U					0.423	17.1	13.0	21.4
	C4	1	54.1							+5.188	ΔT			0.693	13.0	9.9	16.2
	C5	2	2312.9	−535.9	ρ_b	+1123.3	φ_N							0.681	12.1	9.5	15.3
	C6	2	3573.6	−578.7	ρ_b			−90.0	U					0.673	12.2	10.0	15.8
	C7	2	−1002.1	+305.0	ρ_b					+6.607	ΔT			0.713	12.7	10.0	16.1
	C8	2	1703.6			+920.9	φ_N	−58.4	U					0.543	14.7	11.6	18.7
	C9	2	80.7			+917.9	φ_N			+4.213	ΔT			0.878	8.2	6.0	10.2
	C10	2	991.1					−73.5	U	+4.369	ΔT			0.873	6.9	7.1	9.9
	C11	3	2919.7	−522.6	ρ_b	+703.4	φ_N	−54.0	U					0.741	10.4	8.7	13.6
	C12	3	−871.1	+274.8	ρ_b	+908.6	φ_N			+5.502	ΔT			0.895	7.5	6.6	10.0
	C13	3	150.5	+237.2	ρ_b			−72.0	U	+5.490	ΔT			0.886	7.1	6.3	9.5
	C14	3	640.4			+580.3	φ_N	−44.7	U	+4.074	ΔT			0.920	6.1	4.9	7.8
	C15	4	−231.7	+245.2	ρ_b	+585.8	φ_N	−42.9	U	+5.230	ΔT			0.933	6.0	4.5	7.4
Carbonates (n = 15,764)	C16	1	4771.7	−1463.9	ρ_b									0.688	11.6	10.7	15.8
	C17	1	636.6			+2625.3	φ_N							0.797	9.4	8.1	12.4
	C18	1	2014.5					−98.3	U					0.228	19.5	15.5	24.9
	C19	1	−376.7							+6.747	ΔT			0.925	5.9	5.0	7.8
	C20	1	1292.8									+30.9	V_{sh}	0.000	23.0	16.8	28.5
	C21	2	1987.1	−496.4	ρ_b	+1937.1	φ_N							0.821	8.9	7.6	11.7
	C22	2	5138.0	−1769.2	ρ_b			+49.6	U					0.716	11.1	10.0	14.9
	C23	2	−1555.4	+361.4	ρ_b					+8.044	ΔT			0.932	5.6	4.8	7.4
	C24	2	5466.7	−1664.8	ρ_b							−436.5	V_{sh}	0.775	10.0	9.0	13.4
	C25	2	639.9			+2622.5	φ_N	−0.4	U					0.797	9.4	8.1	12.4
	C26	2	−411.5			−115.6	φ_N			+7.005	ΔT			0.925	5.9	5.0	7.8
	C27	2	796.8			+3136.0	φ_N					−578.1	V_{sh}	0.943	4.7	4.4	6.5
	C28	2	−654.7					+23.0	U	+7.199	ΔT			0.933	5.5	4.8	7.3
	C29	2	2194.5					−108.6	U			−210.0	V_{sh}	0.249	19.2	15.2	24.5
	C30	2	−316.7							+7.138	ΔT	−312.8	V_{sh}	0.973	3.5	3.0	4.7
	C31	3	2368.4	−747.0	ρ_b	+1840.8	φ_N	+32.9	U					0.833	8.6	7.2	11.2
	C32	3	−1622.0	+366.7	ρ_b	−163.7	φ_N			+8.427	ΔT			0.933	5.5	4.8	7.4
	C33	3	2247.4	−532.4	ρ_b	+2404.4	φ_N					−585.5	V_{sh}	0.970	3.4	3.1	4.6
	C34	3	−1281.5	+220.4	ρ_b			+15.4	U	+7.840	ΔT			0.935	5.4	4.8	7.2
	C35	3	5728.7	−1902.7	ρ_b			+40.3	U			−413.9	V_{sh}	0.793	9.6	8.5	12.8
	C36	3	−551.7	+71.6	ρ_b					+7.384	ΔT	−304.6	V_{sh}	0.973	3.5	3.0	4.6
	C37	3	−692.0			−122.8	φ_N	+23.0	U	+7.473	ΔT			0.933	5.4	4.8	7.3
	C38	3	926.7			+3041.1	φ_N	−13.8	U			−590.3	V_{sh}	0.946	4.6	4.3	6.3
	C39	3	60.7			+1186.1	φ_N			+4.632	ΔT	−422.5	V_{sh}	0.988	2.3	2.0	3.1
	C40	3	−444.8					+10.4	U	+7.324	ΔT	−298.7	V_{sh}	0.975	3.4	3.0	4.5
	C41	4	−1345.9	+227.0	ρ_b	−150.1	φ_N	+15.2	U	+8.194	ΔT			0.935	5.4	4.8	7.2
	C42	4	2421.2	−649.4	ρ_b	+2349.6	φ_N	+15.4	U			−573.4	V_{sh}	0.973	3.3	2.9	4.4
	C43	4	403.8	−98.0	ρ_b	+1252.7	φ_N			+4.154	ΔT	−439.9	V_{sh}	0.988	2.3	1.9	3.0
	C44	4	−363.7	−28.0	ρ_b			+11.3	U	+7.243	ΔT	−300.8	V_{sh}	0.975	3.4	3.0	4.5
	C45	4	−14.4			+1153.3	φ_N	+5.2	U	+4.795	ΔT	−412.3	V_{sh}	0.988	2.3	2.0	3.0
	C46	5	584.0	−194.4	ρ_b	+1249.6	φ_N	+10.9	U	+4.025	ΔT	−435.9	V_{sh}	0.990	2.2	1.8	2.8

(*Continued.*)

	Eq. #	No. of logs	Bulk-SHC prediction equations [SHC in J (kgK)$^{-1}$]										R^2	Mean	SD	Rms
			b_o	b_{RHOB}		b_{PHIN}		b_U		b_{DT}		b_{VSH}			[per cent]	
Clastic rocks ($n = 151{,}021$)	C47	1	4969.1	−1558.9	ρ_b								0.733	11.8	10.8	16.0
	C48	1	579.9			+3007.8	φ_N						0.913	6.8	5.9	9.0
	C49	1	1968.5					−101.8	U				0.225	21.3	17.6	27.7
	C50	1	−592.0							+7.253	ΔT		0.964	4.3	4.0	5.9
	C51	1	1228.9									+27.2 V_{sh}	0.000	25.1	19.1	31.5
	C52	2	1815.8	−458.5	ρ_b	+2372.0	φ_N						0.936	5.9	5.1	7.8
	C53	2	5370.9	−1893.8	ρ_b			+56.0	U				0.767	11.0	10.1	14.9
	C54	2	−617.7	+7.8	ρ_b					+7.281	ΔT		0.964	4.3	4.0	5.9
	C55	2	5176.2	−1598.4	ρ_b							−206.8 V_{sh}	0.750	11.5	10.4	15.5
	C56	2	939.5			+2813.3	φ_N	−44.5	U				0.952	5.0	4.4	6.6
	C57	2	−411.2			+517.1	φ_N			+6.088	ΔT		0.967	4.2	3.8	5.7
	C58	2	755.3			+3225.8	φ_N					−410.7 V_{sh}	0.975	3.5	3.3	4.8
	C59	2	−507.2					−7.7	U	+7.133	ΔT		0.965	4.3	3.9	5.8
	C60	2	1898.3					−109.8	U			+232.6 V_{sh}	0.245	21.0	17.4	27.3
	C61	2	−517.5							+7.381	ΔT	−196.3 V_{sh}	0.979	3.3	3.1	4.5
	C62	3	708.5	+104.6	ρ_b	+2930.8	φ_N	−50.8	U				0.953	5.0	4.4	6.6
	C63	3	−267.3	−40.4	ρ_b	+549.3	φ_N			+5.872	ΔT		0.967	4.2	3.8	5.7
	C64	3	1820.9	−398.1	ρ_b	+2664.2	φ_N					−392.8 V_{sh}	0.992	2.0	1.9	2.7
	C65	3	−16.6			+1022.3	φ_N	−19.7	U	+4.642	ΔT		0.971	3.9	3.5	5.2
	C66	3	949.1			+3064.6	φ_N	−27.9	U			−336.7 V_{sh}	0.988	2.4	2.2	3.2
	C67	3	59.3			+1535.8	φ_N			+3.989	ΔT	−302.1 V_{sh}	0.994	1.8	1.6	2.4
	C68	3	−551.2					+3.3	U	+7.438	ΔT	−204.2 V_{sh}	0.979	3.3	3.1	4.5
	C69	3	−403.0	−34.7	ρ_b					+7.259	ΔT	−197.7 V_{sh}	0.979	3.4	3.0	4.5
	C70	3	−1029.5	+188.1	ρ_b			−16.3	U	+7.664	ΔT		0.967	4.2	3.9	5.7
	C71	3	6243.8	−2294.3	ρ_b			+106.7	U			−508.2 V_{sh}	0.839	9.2	8.3	12.4
	C72	4	−744.8	+289.8	ρ_b	+1181.7	φ_N	−34.9	U	+5.072	ΔT		0.974	3.7	3.3	5.0
	C73	4	1726.4	−351.6	ρ_b	+2704.8	φ_N	−4.3	U			−383.4 V_{sh}	0.992	2.0	1.9	2.7
	C74	4	891.3	−221.4	ρ_b	+1804.4	φ_N			+2.618	ΔT	−329.5 V_{sh}	0.997	1.3	1.1	1.7
	C75	4	14.3	−206.4	ρ_b			+14.7	U	+6.908	ΔT	−239.8 V_{sh}	0.981	3.2	2.9	4.4
	C76	4	319.3			+1853.0	φ_N	−13.9	U	+3.052	ΔT	−290.9 V_{sh}	0.996	1.4	1.3	1.9
	C77	5	814.6	−182.9	ρ_b	+1840.7	φ_N	−3.6	U	+2.611	ΔT	−321.8 V_{sh}	0.997	1.3	1.1	1.7

Note: Equations are formulated with unstandardized regression coefficients. R^2 is calculated on the synthetic regression set; mean, sd, and rms are calculated on the synthetic testing set. Reduced number of equations for evaporites is induced by non-correlation of VSH to the set of evaporites. For abbreviations see the Appendix D. Multiple regression equations are basically read as: $\alpha = b_0 + b_{RHOB} \cdot RHOB + b_{PHIN} \cdot PHIN + b_U \cdot \underline{U} + b_{DT} \cdot DT + b_{VSH} \cdot VSH$. B_x are unstandardized regression coefficients listed in the appendix, greek letters are well log values. Where a specific regression coefficient is not noted, the associated well-log type is not included in the regression.

APPENDIX D: NOMENCLATURE

Subscripts:			
b	bulk		
fl	fluid		
i	index of point		
lab	laboratory		
ma	matrix		
max	maximum		
mea	measured		
min	minimum		
p	pore		
pred	predicted		
sh	shale		
Tinv	inverted temperature log		
z	depth level		
Statistics:			
ame	arithmetic mean error		
B_{si}	standardised beta coefficients for input variable i		
cv	coefficient of variation		
df	degree of freedom		
F	F-value		
n	number of samples		
p	significance level		
rms	root mean square error		
R^2	coefficient of determination		
SD	standard deviation		
T	tolerance		
Well logging:			
ΔT	sonic interval transit time (DT), [μs m^{-1}]		
γ	(natural) gamma ray (GR), [API]		
$gradT$	temperature gradient, [°C km^{-1}]		
MLR	multiple linear regression		
ϕ_N	neutron porosity (hydrogen index, PHIN), [p.u.]		
NLR	non-linear regression		
p	pressure, [MPa]		
P_e	photoelectric factor log, [pe]		
ρ_b	bulk density (RHO_b), [g cm^{-3}]		
ρ_{ma}	matrix density (RHO_{ma}), [g cm^{-3}]		
RHP, H	radiogenic heat production, [μW m^{-3}]		
SLR	simple linear regression		
SHC, c	specific heat capacity, [J (kg K) $^{-1}$]		
T	temperature, [°C; K]		
TC, λ	thermal conductivity, [W (m K)$^{-1}$]		
TD, α	thermal diffusivity, [m^2 s^{-1}]		
U	photoelectric absorption index, [barns cm^{-1}]		
VP	sonic velocity, [km s^{-1}]		
V_{sh}	volume fraction of shale, [–]		
Other:			
NPB	Northern Permian Basin		
SPB	Southern Permian Basin		
NGB	North German Basin		
DB	Danish Basin		
ML	Molasse Basin		
Conversion:			
Thermal conductivity	1 W (m K)$^{-1}$	=	2.388 mcal (cm s K)$^{-1}$
		=	0.578 Btu (hr ft F)$^{-1}$
Thermal diffusivity	1 m^2 s^{-1}	=	10^4 cm^2 s^{-1}
Specific heat capacity	1 J (kg K) $^{-1}$	=	0.2388 10^{-3} cal (g^{-}°C)$^{-1}$
Sonic interval transit time	1 μs ft^{-1}	=	304.799 kms^{-1}